

## Review

# Physics of the zero- $\bar{n}$ photonic gap: fundamentals and latest developments

Lei Zhou<sup>1,\*</sup>, Zhengyong Song<sup>1</sup>, Xueqin Huang<sup>2</sup> and C.T. Chan<sup>2</sup>

<sup>1</sup> State Key Laboratory of Surface Physics, Key Laboratory of Micro and Nano Photonic Structures (Ministry of Education) and Physics Department, Fudan University, Shanghai 200433, China, e-mail: phzhou@fudan.edu.cn

<sup>2</sup> Physics Department, The Hong Kong University of Science and Technology, Clear Water Bay, Kowloon, Hong Kong, China

\* Corresponding author

Edited by Nader Engheta, University of Pennsylvania, Philadelphia, Pennsylvania, USA

## Abstract

A short overview is presented on the research works related to the zero- $\bar{n}$  gap, which appears as the volume-averaged refraction index vanishes in photonic structures containing both positive and negative-index materials. After introducing the basic concept of the zero- $\bar{n}$  gap based on both rigorous mathematics and numerical simulations, the unique properties of such a band gap are discussed, including its robustness against weak disorder, wide-incidence-angle operation and scaling invariance, which do not belong to a conventional Bragg gap. We then describe the simulation and experimental verifications on the zero- $\bar{n}$  gap and its extraordinary properties in different frequency domains. After that, the unusual photonic and physical effects discovered based on the zero- $\bar{n}$  gap and their potential applications are reviewed, including beam manipulations and nonlinear effects. Before concluding this review, several interesting ideas inspired from the zero- $\bar{n}$  gap works will be introduced, including the zero-phase gaps, zero-permittivity and zero-permeability gaps, complete band gaps, and zero-refraction-index materials with Dirac-Cone dispersion.

**Keywords:** left-handed materials; meta materials; photonic band gaps; photonic crystals.

## 1. Introduction

Over the last several decades, considerable interests appear in employing artificial electromagnetic (EM) materials to control light propagations as desired, which cannot be achieved with naturally existing materials. Such artificial EM materials include photonic crystals (PCs) [1–3] and metamaterials (MTMs) [4–9], operating based on the Bragg and local resonance mechanisms, respectively.

PCs are artificial materials with a periodic modulation on the dielectric constant, which can create a photonic band gap (PBG) via Bragg scatterings, inside which no propagating photonic mode exists [1–3]. PCs have attracted intensive studies in the last two decades due to their unique EM properties and potential applications. The existence of a forbidden frequency band in a PC alters dramatically the properties of light, enabling control of spontaneous emission in quantum devices and light manipulation for photonic information technology [10–12]. However, such a Bragg gap is very sensitive to the periodicity of the system, the incident angle and polarization [transverse electric (TE) wave or transverse magnetic (TM) wave] of the input light, dictated by the Bragg mechanism. As a result, the PBG frequency is inversely proportional to the lattice constant, and thus the size of a PC cannot be made very compact (at least several wavelengths in each dimension) and randomness will destroy the band gap [13–16]. To make photonic devices that are compact in size and robust against disorders, new PBG mechanism needs to be found.

MTMs belong to another class of artificial EM materials [4–9]. These materials are composites consisting of local resonant EM microstructures in subwavelength scales, such that the whole medium can be viewed as a homogeneous one [17] exhibiting *arbitrary* values of electric permittivity  $\varepsilon$  and magnetic permeability  $\mu$ . The much expanded parameter freedom makes MTMs an ideal platform to manipulate EM wave propagations, leading to many interesting phenomena such as negative refraction [8, 9, 18, 19], super imaging [20–23], invisibility cloaking [24–28], and so on. In particular, when both  $\varepsilon$  and  $\mu$  are negative, such a medium is also called a left-handed material (LHM), since  $\vec{E}$ ,  $\vec{H}$ , and  $\vec{k}$  of a plane wave propagating inside it form a left-handed set instead of a right-handed one in a conventional medium. The unusual EM properties of a LHM were first theoretically studied by Veselago in 1968 [4], who found that the direction of energy flow is opposite to that of the wavevector  $k$  inside a LHM, so that an EM wave will be bent negatively when it passes through an interface between a normal medium and a LHM. As a result, such a medium is also said to possess a negative refraction index ( $n$ ) [8, 9, 29]. Other peculiar EM properties of the LHM include reversed Doppler effect [30] and reversed Cherenkov radiation [31]. Veselago's proposal of LHM did not attract immediate attention since it is well accepted that a natural material shows no magnetism at high frequencies [32]. A breakthrough appeared in 1999 when Pendry et al. [6] showed that a split ring resonator (SRR) could provide magnetic responses at any desired frequency. People then

successfully fabricated LHMs by combining SRR and electric resonators such as metallic wires [5], and demonstrated that such a medium can indeed exhibit a negative refractive index [8]. Since then, many efforts were devoted to exploring other intriguing EM manipulation phenomena based on MTMs.

While PCs and MTMs are constructed based on different physical principles and thus the developments of two fields appear quite independent, we notice that there are particular sub-fields that combine the concepts from both sides and then new physics emerge from the interplays between two physical principles. For example, employing PCs with anomalous dispersions to mimic the negative refraction behaviors of LHMs attracted much attention in early developments of MTMs [33–35]. On the other hand, PCs built with LHMs were found to exhibit many unusual properties. In particular, it was first discovered in [36] that a new type of PBG called zero- $\bar{n}$  gap arises in a PC consisting of both right-handed materials (RHMs) and LHMs. Such a zero- $\bar{n}$  gap exhibits many unusual physical properties that do not exist in a conventional Bragg PBG, such as central-frequency scaling invariance and robustness against weak disorders. Later, many other unconventional physical properties of the zero- $\bar{n}$  gap were discovered, and the existence of such a special PBG was experimentally verified in different frequency regimes. More recently, several interesting ideas were inspired from the zero- $\bar{n}$  gap works, resulting in new sub-branches in photonic research.

In this paper, we will briefly review the fundamental physics and latest developments of the zero- $\bar{n}$  gap research. We have no intention to make this paper a comprehensive overview on the development of the whole sub-field, but rather try to make it concise and idea-inspiring. This review is organized as follows. We first introduce the basic concept and some preliminary properties of the zero- $\bar{n}$  gap in Section 2, and then summarize in Section 3 the available efforts from both full-wave simulations and experiments on verifying the zero- $\bar{n}$  gap and its extraordinary physical properties. Section 4 is devoted to reviewing the unusual physical effects discovered based on the zero- $\bar{n}$  gap materials, and Sections 5 and 6 summarize some interesting ideas inspired from the zero- $\bar{n}$  gap research. We conclude this review in Section 7.

## 2. Basic concept and extraordinary properties of the zero- $\bar{n}$ gap

We first present a proof that in a one-dimensional (1D) layered stack containing both positive- and negative- $n$  materials,  $\bar{n}=0$  implies the existence of a PBG [36]. Consider a 1D layered PC described by a periodic frequency-dependent permittivity  $\varepsilon(x+a)=\varepsilon(x)$  and permeability  $\mu(x+a)=\mu(x)$ , where  $a$  is the lattice constant. The dispersion relation  $\omega(k)$  of such a PC can be obtained by solving the following equation,

$$-\frac{Z(x)}{n(x)} \frac{d}{dx} \left[ \frac{1}{Z(x)n(x)} \frac{dE(x)}{dx} \right] = \left( \frac{\omega}{c} \right)^2 E(x) \quad (1)$$

where  $c$  is the speed of light,  $n(x)=\sqrt{\varepsilon(x)}\sqrt{\mu(x)}$  and  $Z(x)=\frac{\sqrt{\mu(x)}}{\sqrt{\varepsilon(x)}}$  are respectively the refraction index and impedance at frequency  $\omega$ . Imposing the periodicity constraint  $\vec{E}(x+a)=e^{ika}\vec{E}(x)$ , we find that the dispersion relation is determined by

$$\text{Tr}[T(\omega)]=2\cos ka, \quad (2)$$

where  $T(\omega)$  is a  $2 \times 2$  transfer matrix. For a double-layer unit-cell, a simple calculation yields

$$\text{Tr}[T(\omega)]=2\cos\left(\frac{\bar{n}\omega a}{c}\right) - \left(\frac{Z_1+Z_2}{Z_2+Z_1}-2\right)\sin(n_1d_1\omega/c)\sin(n_2d_2\omega/c), \quad (3)$$

where  $n_i$ ,  $Z_i$ ,  $d_i$  are, respectively, the refractive index, impedance, and thickness of the  $i$ th layer. Clearly, the first term in Eq. (3) represents the solution in a homogeneous medium with average refractive index  $\bar{n}=(n_1d_1+n_2d_2)/a$ , while the second term is responsible for gap opening if there is an impedance mismatch. For the special case of matched impedance ( $Z_1=Z_2=Z_0$ , a constant), the dispersion relation is given by  $ka=\bar{n}\omega a/c$ . In general case ( $Z_1 \neq Z_2$ ), when

$$\bar{n}\omega a/c = m\pi \quad (m \in \text{integers}), \quad (4)$$

Eq. (3) becomes

$$|\text{Tr}(T)| = \left| 2 + \left( \frac{Z_1+Z_2}{Z_2+Z_1} - 2 \right) \sin^2(n_1d_1\omega/c) \right| \geq 2. \quad (5)$$

Except that

$$n_1d_1\omega/c = p\pi \quad (p \in \text{integers}), \quad (6)$$

Eq. (5) implies that Eq. (2) has no real solution for  $k$ , indicating the opening of a band gap. Equation (4) is the familiar Bragg condition, which can have multiple solutions for conventional PBG materials. However, if we mix both positive and negative- $n$  materials to form a periodic structure, there is an extra possibility that

$$\bar{n}=0, \quad (7)$$

which also leads to Eq. (5) and thus a spectral gap. This new type of band gap differs fundamentally from the usual Bragg gap, as we shall demonstrate in the subsequent sections.

The  $\bar{n}=0$  condition for the spectral gap is not limited to a periodic AB stacking, but is generally true in 1D periodic systems. Equation (1) is equivalent to two coupled first order differential equations,

$$\begin{aligned} \frac{dE_+(x)}{dx} e^{i\frac{\omega}{c}\int_0^x ndx'} &= -\frac{dE_-(x)}{dx} e^{i\frac{\omega}{c}\int_0^x ndx'} \\ &= \frac{1}{2Z} \frac{dZ}{dx} \left[ E_+(x) e^{i\frac{\omega}{c}\int_0^x ndx'} - E_-(x) e^{-i\frac{\omega}{c}\int_0^x ndx'} \right], \end{aligned} \quad (8)$$

where the  $E$  field is decomposed as

$$E(x) = E_+(x)e^{i\frac{\omega}{c}\int_0^x ndx'} + E_-(x)e^{-i\frac{\omega}{c}\int_0^x ndx'}. \quad (9)$$

For periodic systems, we look for Bloch solutions satisfying

$$E_+(a)e^{i\frac{\omega}{c}\bar{n}a} = e^{ika}E_+(0), \quad E_-(a)e^{-i\frac{\omega}{c}\bar{n}a} = e^{ika}E_-(0). \quad (10)$$

Suppose there is a certain frequency  $\omega_0$  that  $\bar{n}(\omega_0)=0$ . If  $Z(x)=Z_0$  (perfect impedance match), Eq. (8) has two degenerate solutions at  $\omega_0$ , both with  $k=0$  and the E-field is given by

$E^{(0)}(x) = \alpha e^{i\frac{\omega_0}{c}\int_0^x ndx'} + \beta e^{-i\frac{\omega_0}{c}\int_0^x ndx'}$ . When  $Z(x)=Z_0+\Delta Z(x)$ , with  $\Delta Z(x)$  arbitrary but periodic, solving Eq. (8) [with Eq. (10)] by taking both  $E(x)$  and  $k$  up to first order in  $\Delta Z(x)$ , we find that

$$k = \pm i \frac{1}{a} \int_0^a \frac{1}{2Z_0} \frac{d\Delta Z(x)}{dx} e^{2i\frac{\omega_0}{c}\int_0^x ndx'} dx. \quad (11)$$

Since  $k$  is imaginary, there must be a gap at  $\omega_0$  if  $\bar{n}(\omega_0)=0$ .

To illustrate the basic ideas, we first consider a simple 1D system composed by *non-dispersive* positive- and negative- $n$  layers with structural and material parameters (given in the caption of Figure 1) satisfying  $\bar{n}=0$ . The dispersion relationship  $\omega(k)$  and the transmittance through a 32-unit slab as functions of frequency are shown in Figure 1. The condition  $\bar{n}=0$  is satisfied for all frequencies in this model system. The numerical solution shows that the photonic gap covers all frequencies (no transmission and  $k$  purely imaginary) except for singular frequency points satisfying Eq. (6). However, we show below that these singular frequency points will disappear if  $n$  is frequency dependent. For those frequencies satisfying  $\bar{n}(\omega_0)=0$  and Eq. (6), we have  $Tr[T(\omega)]=2$ , and near  $\omega_0$ ,

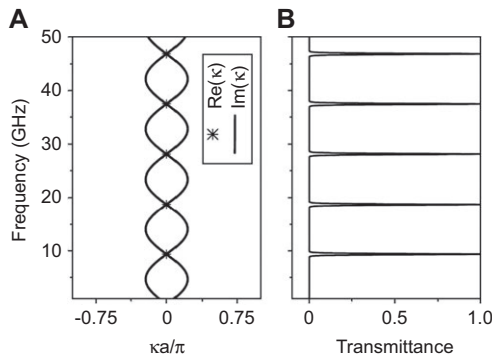


**Figure 1** (A) Dispersion relationship of a photonic crystal with unit cell consisting of one layer of air (thickness=16 mm) and one layer of negative- $n$  material ( $\epsilon=-8, \mu=-2$ , thickness=4 mm). (B) Transmittance through a 1D photonic crystal slab consisting of 32 such unit cells. Reproduced from Ref. [36] with the permission of American Physics Society.

$$Tr(T) \approx 2 - \left( Z_1 \frac{dn_1\omega}{d\omega} \Big|_{\omega_0} d_1 + Z_2 \frac{dn_2\omega}{d\omega} \Big|_{\omega_0} d_2 \right) \times \left( \frac{1}{Z_1} \frac{dn_1\omega}{d\omega} \Big|_{\omega_0} d_1 + \frac{1}{Z_2} \frac{dn_2\omega}{d\omega} \Big|_{\omega_0} d_2 \right) \times \left( \frac{\omega - \omega_0}{c} \right)^2, \quad (12)$$

which is always less than 2 if we enforce the general condition on the dispersion,  $\frac{d\varepsilon(\omega)\omega}{d\omega} > 0$  and  $\frac{d\mu(\omega)\omega}{d\omega} > 0$ ; which ensures

a positive definite energy density. Equation (12) implies that we have a gap with zero width near  $\omega_0$ . Therefore, it is unlikely to realize a transmission band inside the zero- $\bar{n}$  gap (like in Figure 1) in realistic systems, when materials' dispersions are correctly taken into account. However, the transmission resonance [Eq. (6)] and the zero- $\bar{n}$  gap can coexist in the same system, but observable at different incident angles. The interplay between these two effects leads to many new physics, as shown in Section 4.

The zero- $\bar{n}$  gap possesses some unique properties that distinguish itself from a Bragg gap. In studying the peculiar physical properties of such a gap, one should always bear in mind that the frequency dispersion of the LHM must be carefully taken into account, since otherwise the predicted effects might be unphysical. Li et al. considered a 1D system with alternate layers of air and dispersive negative- $n$  materials [36] with effective  $\varepsilon(\omega)$  and  $\mu(\omega)$  given by

$$\varepsilon(f) = 1 + \frac{5^2}{0.9^2 - f^2} + \frac{10^2}{11.5^2 - f^2}, \quad \mu(f) = 1 + \frac{3^2}{0.902^2 - f^2}, \quad (13)$$

where  $f$  is the frequency measured in GHz. Numerical values of  $\varepsilon(\omega)$  and  $\mu(\omega)$  are given in Figure 2(A). The band structure is shown in Figure 2(B), while the solid line in Figure 2(C) gives the transmittance through a stack of 16 unit cells. The band structure and the transmittance clearly show two band gaps. The  $\bar{n}$  of the system (air plus the negative- $n$  material) is zero at 2.3 GHz, and a gap does open at that frequency. Another gap is clearly shown at about 8 GHz, which originates from Bragg scattering.

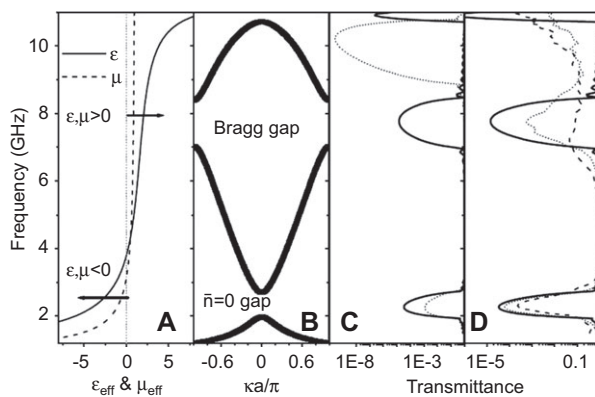
A Bragg gap is an intrinsic consequence of periodicity, and the gap frequency is tied with the size of the unit-cell. When we scale the unit-cell size by a factor, a Bragg gap will shift in frequency accordingly, in order to make Eq. (4) still satisfied. However, the zero- $\bar{n}$  gap is independent of periodicity and should remain invariant with scaling. In fact, the zero- $\bar{n}$  gap can be regarded as the zero-th order Bragg gap [i.e.,  $m=0$  in Eq. (4)]. The uniqueness of such a special Bragg gap is that, as we scale the unit cell by a factor, the phase accumulation of a wave passing through the *scaled* unit cell is still zero, which ensures the gap opening condition Eq. (4) satisfied for the scaled system. Such a property only exists in a composite medium with both positive- and negative- $n$  components, so that phase accumulations through different parts can exactly cancel each other. Apparently, such phase cancellation is insensitive to rescaling the whole structure, which is not the case for a conventional Bragg gap. Solid line in Figure 2(C) is the transmittance corresponding to the band structure in

Figure 2(B); while dotted line is the transmittance through the same system but with lattice constant  $a$  scaled by a factor of  $2/3$ . The Bragg gap that was originally near 8 GHz shifts upwards in frequency, as expected. However, the zero- $\bar{n}$  gap remains unchanged at 2.3 GHz, because the change of scale does not influence the value of  $\bar{n}=0$ . This peculiar property is of particular importance to realize ultra-compact photonic devices.

A Bragg gap is sensitive to deviation from periodic order. Figure 2(D) compares the transmittances through several 16 unit-cell stacks possessing different degrees of disorder. Solid line corresponds to a perfectly ordered stack, while dotted and dashed lines correspond to the transmission through stacks with thickness deviation (random uniform deviate) of  $\pm 3$  and  $\pm 6$  mm, respectively, each ensemble averaged over 24 realizations. As expected, the Bragg gap is destroyed by strong disorder, but the zero- $\bar{n}$  gap survives. The robustness of the zero- $\bar{n}$  gap comes from the fact that the  $\bar{n}(\omega)=0$  solution remains invariant under disorder that is symmetric (+ and - deviations are equally probable).

The zero- $\bar{n}$  gap was found to be an omnidirectional one, in the sense it is rather insensitive to the incident angle and polarization of the input wave. In contrast to Ref. [36] where only the normal incidence case was considered, Jiang et al. [37] studied how a zero- $\bar{n}$  gap and a Bragg gap evolve as incident angle and polarization change in a carefully designed 1D PC. The results were reproduced in Figure 3 where the upper band gap was identified as a conventional Bragg gap and the lower one the zero- $\bar{n}$  gap. While a Bragg gap varies dramatically as a function of incident angle and polarization, and even disappears in certain situations, the zero- $\bar{n}$  gap remains nearly invariant in the whole angle range studied.

The physical properties of a localized defect mode inside the zero- $\bar{n}$  gap were also found very unusual. By inserting a



**Figure 2** (A) Effective  $\epsilon$  and  $\mu$  of the negative- $n$  material, as given by Eq. (13). (B) Dispersion relationship of a photonic crystal with alternate layers of air (12 mm thick) the negative- $n$  material (6.0 mm thick) with material parameter as shown in (A). (C) Solid line: Transmittance through 16 unit cells, corresponding to the band structure in (B). Dotted line: Transmittance when the lattice constant is scaled by  $2/3$ . (D) Transmittance through 16 unit cells, with various degree of disorder in thickness. Reproduced from Ref. [36] with the permission of American Physics Society.

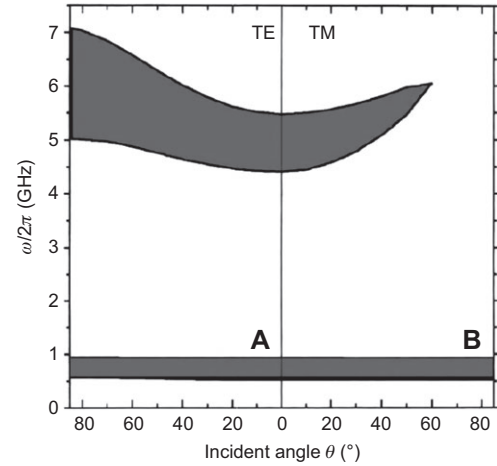


**Figure 3** Evolutions of a conventional Bragg gap (upper black region) and a zero- $\bar{n}$  gap (lower black region) as functions of incident angle and polarization, calculated for a 1D PC containing alternative stacking of homogeneous positive- $n$  and negative- $n$  slabs with structural and material details recorded in Ref. [37]. Reproduced from Ref. [37] with the permission of American Institute of Physics.

defect layer into a PC, defect modes can be induced inside both zero- $\bar{n}$  and Bragg gaps. It was shown in Ref. [37] that the defect mode inside the zero- $\bar{n}$  gap remains invariant with the scaling of non-defect part, while the defect mode inside the Bragg gap shifts greatly in frequency with scaling. On the other hand, when the incident angle increases from  $0^\circ$  to  $30^\circ$ , the defect mode inside the zero- $\bar{n}$  gap remains nearly invariant, while the defect mode inside the Bragg gap changes quickly (see Figure 4). These unusual physical behaviors of defect modes are dictated by the unusual properties of the zero- $\bar{n}$  gap, which have already been illustrated.

### 3. Realizations of the zero- $\bar{n}$ gap: simulations and experiments

In the last section, we have summarized the peculiar EM properties of the zero- $\bar{n}$  gap predicted based on *model* systems with pre-assumed effective (frequency dependent)  $\epsilon$  and  $\mu$ . In this section, we briefly review the existing efforts, from both full-wave simulations and experiments, to verify those highly unusual properties of the zero- $\bar{n}$  gap based on *realistic* structures.

Li et al. [36] first designed a structure that exhibits such an unconventional stop band with help of finite-difference-time-domain (FDTD) simulations. A building block for the negative- $n$  material is shown in Figure 5, in which the rectangular metallic SRR on the left and right gives negative  $\mu$ , while the metal fork in the middle gives negative  $\epsilon$ . The basic building block is replicated to tile the  $\vec{E}-\vec{H}$  plane to form a negative- $n$  slab, whose effective  $\epsilon(\omega)$  and  $\mu(\omega)$  were derived from the FDTD simulated transmission/reflection spectra. Figure 6(A) shows that both  $\epsilon_{eff}$  and  $\mu_{eff}$  are negative within a frequency window 4.1–4.8 GHz, demonstrating that the material is a

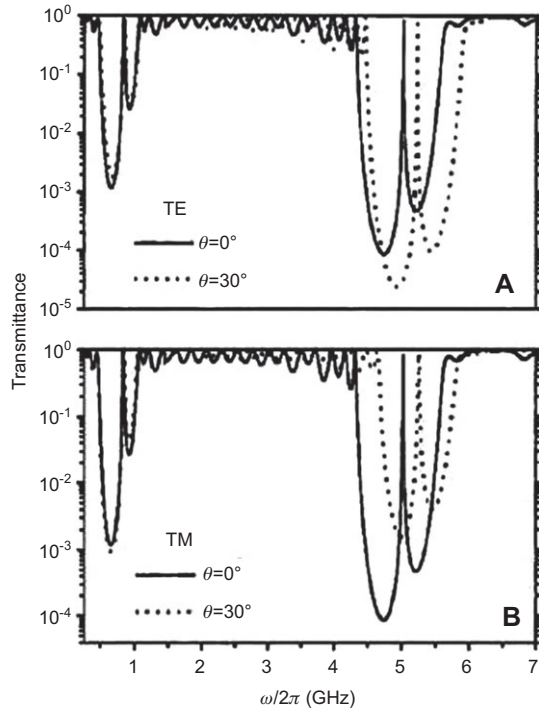


**Figure 4** Transmittance through a doped 1D PC containing both positive- $n$  and negative- $n$  slabs (see Ref. [37] for the structural and material parameters), calculated at different incident angles and polarizations. Reproduced from Ref. [37] with the permission of American Institute of Physics.

negative- $n$  one. A 1D PC is formed by repeating the unit cell consisting of this negative- $n$  slab and a 7-mm air gap (serving as the positive- $n$  medium). Li et al. employed FDTD simulations to calculate the transmission spectrum for a 16-unit-cell slab with microstructures fully taken into account. The results are plotted as open circles in Figure 6(C). They also calculated the band structure [Figure 6(B)] of the 1D PC and the transmittance through a 16-unit-cell slab [solid line in Figure 6(C)], assuming that the negative- $n$  material is a homogeneous slab described by  $\epsilon_{\text{eff}}(\omega)$  and  $\mu_{\text{eff}}(\omega)$ . Both the band structure [Figure 6(B)] and the transmission spectra [Figure 6(C)] clearly show two band gaps, where the upper gap was unambiguously identified as the zero- $\bar{n}$  gap since  $\bar{n}=0$  at about 4.5 GHz.

Subsequently, Yuan et al. [38] experimentally demonstrated the existences of the zero- $\bar{n}$  gap in microwave regime, and verified some of its key properties. As shown in Figure 7(A), the double-S structure was chosen to play the role of LHM [39] (with thickness  $b_1$ ) while the dielectric substrate without metallic structure was chosen as the RHM (with thickness  $b_2$ ), and EM waves were fed along the  $x$  direction with  $\vec{E} \parallel \hat{z}$ . Four different samples were experimentally measured [Figure 7(B)]. Samples A and B have the same  $b_2$  but different  $b_1$ . For samples C and D,  $b_1$  and  $b_2$  are doubled with respect to samples A and B, respectively. Measured transmission spectra for samples A and C are shown as solid lines in Figure 8(A) and 8(B), respectively. Figure 8(A) shows that two gaps occur at  $\sim 11.5$  GHz and  $\sim 15$  GHz for sample A, which were identified

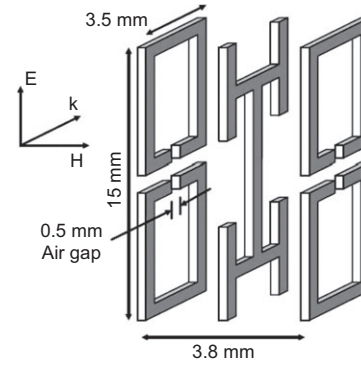


**Figure 5** Structural details of the negative- $n$  material. Reproduced from Ref. [36] with the permission of American Physics Society.

as a (-1 order) Bragg gap and the zero- $\bar{n}$  gap by numerical calculations, respectively. Transmission spectrum for sample C [Figure 8(B)] shows that, when the period of the RHM-LHM superlattice is doubled, the Bragg gap shifts away from the frequency of interests but the zero- $\bar{n}$  gap remains almost unchanged. This was not only the first experimental illustration of the zero- $\bar{n}$  gap, but also unambiguously demonstrated the most important property of the zero- $\bar{n}$  gap that its working frequency is independent of the periodicity.

Zhang et al. [40] chose the microstrip transmission lines (TL) to experimentally demonstrate the existence of the zero- $\bar{n}$  gap. As shown in Figure 9, the authors combined ordinary TL units (denoted as “A” representing a positive- $n$  material) and composite right/left-handed TL unit (denoted as “B” representing a negative- $n$  material) to form a series of 1D PCs defined by  $(A_m B_n)_p$ , where  $m$  ( $n$ ) denotes the number of A (B) unit inside a unit cell and  $p$  the total number of unit cells inside the PCs. The measured and simulated transmission

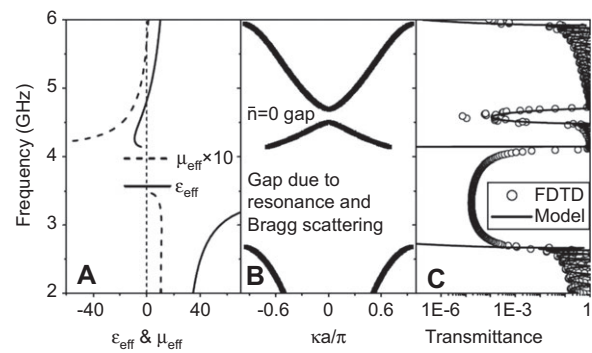


**Figure 6** (A)  $\epsilon_{\text{eff}}$  and  $\mu_{\text{eff}}$  as functions of frequency of the negative- $n$  material. (B) Band structure for a photonic crystal with alternating layers of air (7 mm thick) and the designed negative- $n$  material [thickness=3.5 mm,  $\epsilon_{\text{eff}}$ ,  $\mu_{\text{eff}}$  shown in (A)]. (C) Transmittance through a slab consisting of 16 unit cells with details described above, through direct FDTD simulation (open circles) and material properties represented by  $\epsilon_{\text{eff}}$  and  $\mu_{\text{eff}}$  (solid line). Reproduced from Ref. [36] with the permission of American Physics Society.

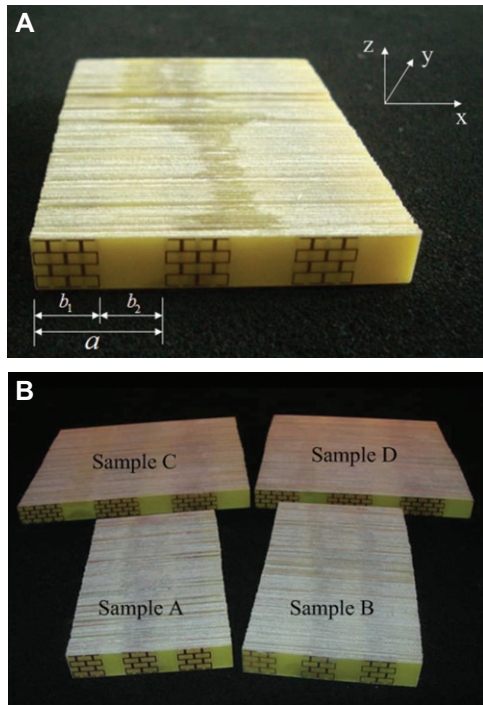


**Figure 7** Pictures of the samples used in microwave experiments to verify the existence of zero- $\bar{n}$  gaps. (A) One typical sample behaving as a 1D LHM/RHM PC. (B) Samples of the same sort used in a series of verification experiments. Reproduced from Ref. [38] with the permission of Optical Society of America.

spectra for such 1D PCs are reproduced in Figure 10, from which a common gap centered at  $\sim 1.9$  GHz can be found in all PCs studied. By carefully examining the 1D PCs containing A or B units only, the authors were able to retrieve the effective parameters of such units and found that the common gaps centered at  $\sim 1.9$  GHz are just the zero- $\bar{n}$  gaps. Figure 10 already demonstrated that the center frequencies of such zero- $\bar{n}$  gaps are independent of the lattice scaling, and the authors further proved that such zero- $\bar{n}$  gaps are rather robust against disorder since they found experimentally that such

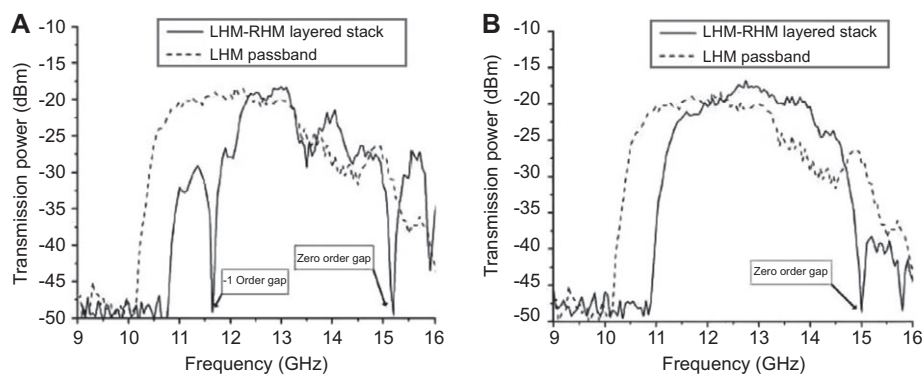


**Figure 8** Measured transmission spectra (solid lines) through samples (A) A and (B) C, with material/structural details recorded in Ref. [38]. Dashed lines represent the measured transmission spectra through the double-S shaped LHM. Reproduced from Ref. [38] with the permission of Optical Society of America.

gaps can even appear in PCs with quasi-periodicity. We will come back to this point in the next section.

In 2009, Kocaman et al. [41] presented the first experimental observation of the zero- $\bar{n}$  gap in near infrared (IR) regime. It is highly challenging even today to fabricate high-quality transparent LHMs at high frequencies, and the authors skillfully designed a PC with anomalous band structure to *emulate* an LHM [42] and then stack such PCs and positive- $n$  dielectric materials to form a 1D superlattice. Actually, in 2006, Panoui et al. [43] already theoretically proposed the idea of combining normal PCs and negative-refraction PCs to realize a 1D superlattice exhibiting a zero- $\bar{n}$  gap, but such an idea was only experimentally realized in 2009 [41]. A scanning electron microscope (SEM) image of the fabricated sample was reproduced in Figure 11(A), where the period of the superlattice is defined as  $\Lambda = d_1 + d_2$  with  $d_1$  and  $d_2$  being the thicknesses of the *effective* LHM and positive- $n$  layers. The designed PC layer possesses a negative index for TM-polarized input wave (magnetic field parallel to top surface of PC) in the wavelength range of 1485.1–1556.4 nm, as illustrated by its photonic band structure depicted in Figure 11(B). The authors first employed full wave simulations to carefully study the PBG properties of such systems, and identified the existence of a zero- $\bar{n}$  gap that is independent of the superlattice constant  $\Lambda$ . Figure 12(A) and (B) show the measured and simulated transmission spectra for two designed/fabricated structures (with different  $d_2/d_1$ ). Two distinct gaps were observed, of which the gaps around 1550 nm were identified as the zero- $\bar{n}$  gaps by comparing with numerical analyses, while the others were found as Bragg gaps. Figure 12(C) compares the transmission spectra for a series of samples, each with the same super cell structure as Figure 12(A) but with increasing stack numbers. The intensity contrast of the zero- $\bar{n}$  gap increases with increasing number of superperiods. Moreover, in contrast to Bragg gaps, experiments showed that the zero- $\bar{n}$  gap is surprisingly robust against nanofabrication-induced disorder, which is another unique character of the zero- $\bar{n}$  gap.

Zero- $\bar{n}$  material has also been realized by Mocella et al. [44] in the near-IR regime using alternating stripe layers of negatively refracting (silicon-based PCs with  $n_{eff} \approx -1$ ) and

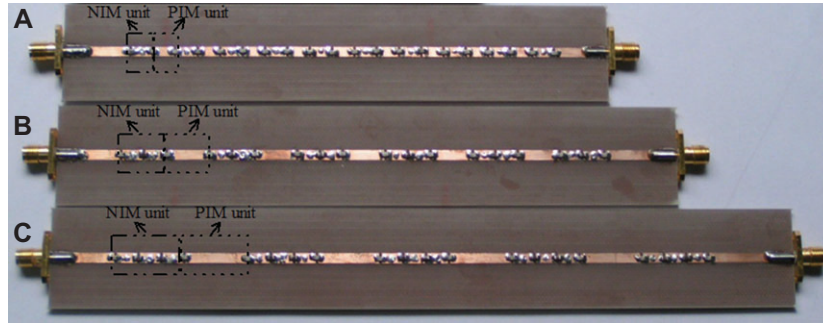


**Figure 9** Photographs of the proposed PCs defined by (A)  $(AB)_{10}$ , (B)  $(A_2B_2)_6$  and (C)  $(A_3B_3)_5$  composed by positive- $n$  materials (microstrip TL units) and negative- $n$  materials (CRLH TL units). Reproduced from Ref. [40] with the permission of Institute of Physics.

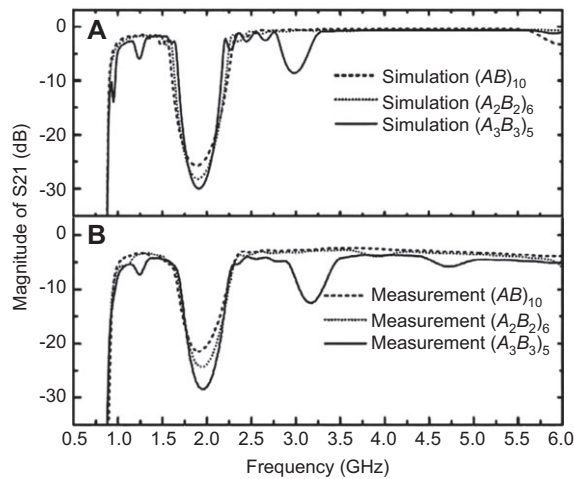


**Figure 10** (A) Simulated and (B) measured  $S$ -parameters of PCs  $(AB)_{10}$ ,  $(A_2B_2)_6$  and  $(A_3B_3)_5$  with material and structural details recorded in Ref. [40]. Reproduced from Ref. [40] with the permission of Institute of Physics.

positively refracting (air,  $n=1$ ) materials. The authors called such composite materials “quasi-zero-average-index (QZAI) metamaterial”, and a zero- $\bar{n}$  gap was observed. The QZAI material can collimate a beam of near-IR light for millimeter distances [44].

#### 4. Unusual physical effects related to zero- $\bar{n}$ gaps

Stimulated by the highly unusual properties of the zero- $\bar{n}$  gap, many exciting photonic and physical effects were subsequently discovered. In this section, we briefly review such works, including beam manipulations, nonlinear phenomena, and extensions to quasi-periodic systems.

##### 4.1. Beam manipulations using zero- $\bar{n}$ gap materials

For 1D PCs composed by RHM and LHM layers (placed at the  $xy$  plane) with thicknesses  $a$  and  $b$  and refractive indexes  $n_r$  and  $n_l$ , Shadrivov et al. [45] explored the extraordinary

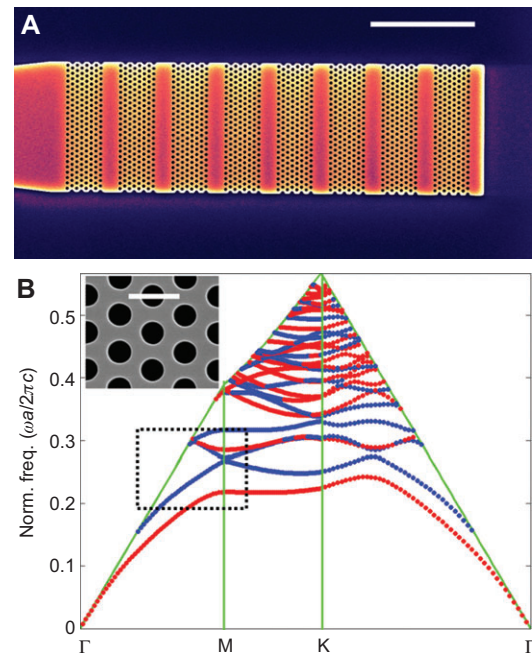


**Figure 11** (A) SEM image of a fabricated sample with eight stacks, whose PC slab layer has a length of  $d_l=3.5\sqrt{3}a$ . Scale bar: 5  $\mu\text{m}$ . (B) Calculated photonic band structure of the fabricated PC slab waveguide with  $r=0.290a$  and  $t=0.762a$  ( $a=420$  nm). The TM-like [TE-like] photonic bands are depicted in blue (darker) [red (lighter)]. Inset: SEM image of the PC region of the fabricated superlattice. Scale bar: 500 nm. Reproduced from Ref. [41] with the permission of American Physics Society.

angular-dependences of their transmission properties, by considering the interplays between the zero- $\bar{n}$  gap effect [Eq. (7)] and the transmission resonance [Eq. (6)]. As proved in Section 2, when the 1D PC is designed to let two conditions Eqs. (6–7) satisfied simultaneously at a particular frequency  $\omega_0$ , the zero- $\bar{n}$  gap will be closed at normal incidence. However, at off-normal incidence (with a non-zero  $k_x$ ), the zero- $\bar{n}$  gap can reopen at some frequencies, resulting in a dispersion diagram as shown in Figure 13(A) with gap region denoted by gray color. The dispersion diagram can be dramatically changed if

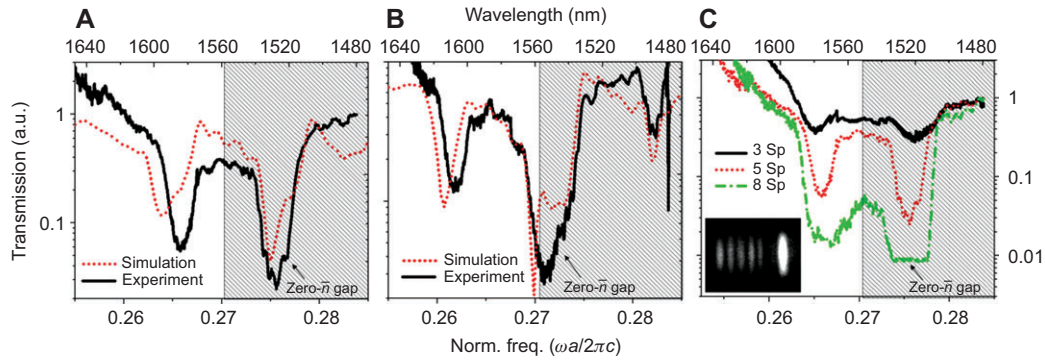


**Figure 12** (A) Measured transmission for a superlattice with  $d_2/d_1=0.746$ , with 7 unit cells in the negative- $n$  PC layers and 5 superperiods; for comparison, results of numerical simulations are also shown. (B) The same as in (A), but for a superlattice with  $d_2/d_1=0.794$ . (C) Measured transmission for a superlattice with  $d_2/d_1=0.746$ , with 3, 5, and 8 superperiods and 7 unit cells in the negative- $n$  PC layers. Both gaps become deeper as the number of stacks increases. Inset: Example of near-infrared top view image of 3 superperiods, under transmission measurement at 1550 nm. In all plots, the shaded region illustrates the negative- $n$  region. Reproduced from Ref. [41] with the permission of American Physics Society.

the transmission condition  $n k_0 \cos \theta a = \pi$  [the off-normal version of Eq. (6)] is satisfied at an oblique angle  $\theta$ , as depicted in Figure 13(B). At the frequency denoted by two dashed lines in Figure 13, insets show the transmission coefficients in the  $k_x$ - $k_y$  plane for two systems. Thus, one can design a system which is transparent only at the desired incident angles. In

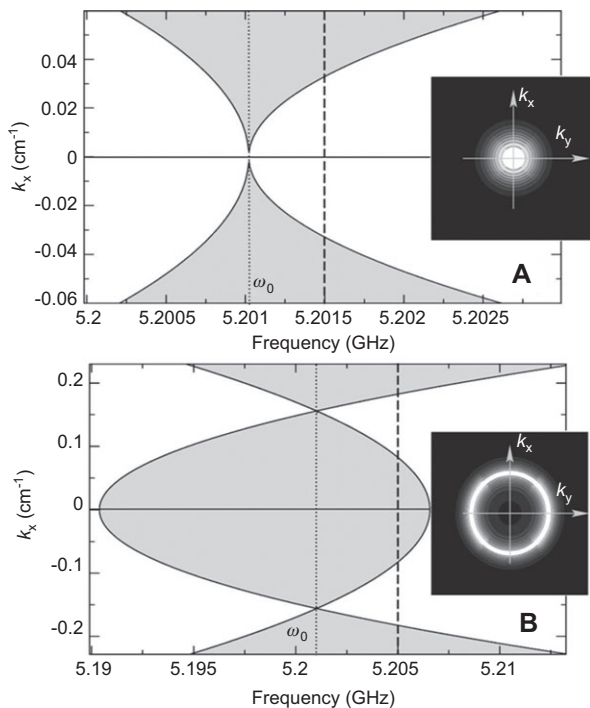


**Figure 13** Band gap structure on the parameter plane ( $\omega$ ,  $k_x$ ) with gaps shaded. (A) Transmission band corresponds to a normal incidence. (B) Transmission band corresponds to an oblique incidence. Dotted line denotes the frequency  $\omega_0$ . Insets show the beam transmission coefficients at the frequencies marked by dashed lines. Reproduced from Ref. [45] with the permission of American Institute of Physics.

addition, structures with more complicated transmission properties (with multiple rings in the transmission pattern) can be also obtained. These systems can be employed to dramatically reshape the wave-fronts of incident beams passing through them, leading to many interesting wave-front patterns [45].

Kivshar's group continued to utilize the interplays between the zero- $\bar{n}$  gap and the transmission resonances in *chirped* 1D PCs [see Figure 14(A)] to achieve other beam manipulation effects, such as Bloch oscillations [46] and Beam curling [47]. The physics is very simple. For a series of 1D periodic systems with parameters satisfying the  $\bar{n}=0$  condition at normal incidence, the authors calculated the band gap diagram on the ( $\Lambda$ ,  $k_y$ ) plane with  $\Lambda$  being the lattice constant and  $k_y$  the parallel wavevector. Figure 14(B) shows that the system exhibits a gap at normal incidence (i.e.,  $k_y=0$ ). However, the transmission resonance condition [e.g., Eq. (6)] can be met in some particular off-normal situations, generating the white regions in Figure 14(B). Such an unusual band gap diagram on the ( $\Lambda$ ,  $k_y$ ) plane can be translated to an effective band gap diagram on the ( $z$ ,  $k_y$ ) plane for a *non-uniform* PC with position-dependent (local) periodicity  $\Lambda(z)$  [see Figure 14(A)]. If such a mapping is valid, one may find from Figure 14(B) that there are narrow transmission bands (white areas) sandwiched between zero- $\bar{n}$  gaps (black areas), which are precisely the conditions to achieve Bloch oscillations of EM waves. Indeed, Figure 15 shows one typical example of such predicted Bloch oscillations, where the EM wave is bounced back and forth by two zero- $\bar{n}$  gap boundaries. The authors predicted three different types of Bloch oscillations in such structures, one of which is associated with coupling between surface waves, which does not exist in other systems. In addition, they also predicted more fascinating beam manipulation effects such as beam curling, in large systems satisfying certain conditions [47].

## 4.2. Nonlinear effects related to the zero- $\bar{n}$ gap

Several groups studied the nonlinear optical effects [48–51] in zero- $\bar{n}$  systems, which were again found rather

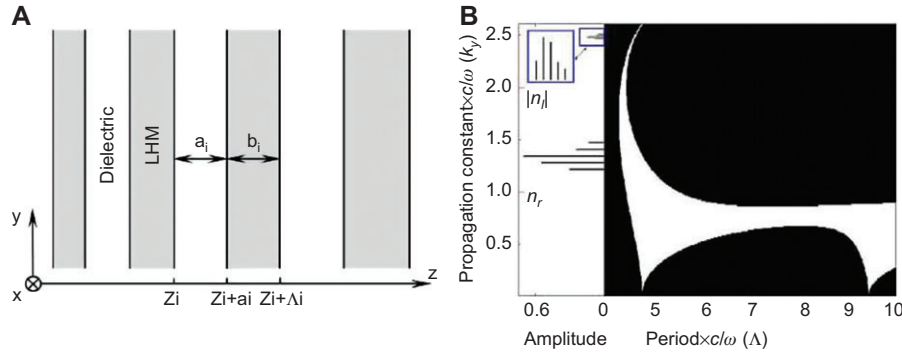


**Figure 14** (A) Schematic of linearly chirped 1D structure with alternating layers of negative- $n$  MTM and conventional dielectric. (B) Bandgap diagram for the TE-polarized waves in structure with alternating dielectric ( $\epsilon_r = \mu_r = 1$ ) and MTM ( $\epsilon_r = -5, \mu_r = -0.8$ ) in case of zero average refractive index. Black and white areas correspond to gaps and bands, respectively. Two spectra of the excited Bloch oscillations are shown on the left. The inset shows a magnified part of the spectrum. Reproduced from Ref. [46] with the permission of Optical Society of America.

intriguing. Replacing one LHM layer in a 1D LHM/RHM PC by a defect layer with Kerr-type nonlinear response  $[\epsilon_r(t) = 1 + \chi^{(1)} + \chi^{(3)} |\vec{E}(t)|^2]$ , Feise et al. [48] theoretically studied the optical responses of such a system in both linear (low-field) and nonlinear (high field) regimes. Defect-induced transmissions were found inside both zero- $\bar{n}$  and Bragg gaps, which sensitively depended on the input power. Such dependences could lead to optical hysteresis and bistability, which may find applications in all-optical logical devices [52]. The authors found that, for defect-induced transmission related to the zero- $\bar{n}$  gap, the optical bistability is rather robust against the defect-layer offset and the difference between switch-up and switch-down threshold is much larger, in sharp contrast to those related to a conventional Bragg gap [48].

Different from [50] where only the defect layer is formed by nonlinear material, Hegde and Winful [49] studied the case where *all* RHM layers in the 1D LHM/RHM PC are formed by nonlinear Kerr materials. No defect-induced transparency exists here since the system is still perfectly periodic.

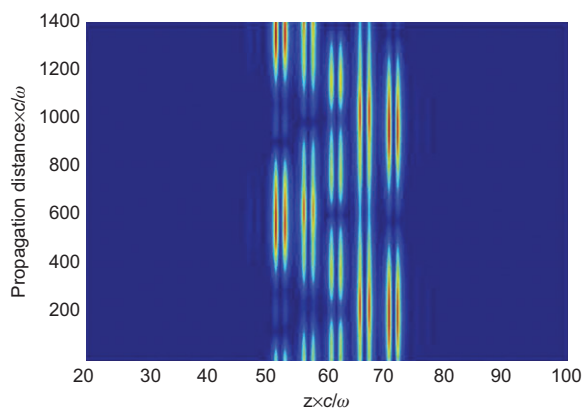


**Figure 15** Field distribution in the case of surface-wave-assisted Bloch oscillations. The Wannier-Stark ladder appears for the propagation constants centered around  $k_{y0} = 2.47$ , normalized period is  $L_y = 820$ . Reproduced from Ref. [46] with the permission of Optical Society of America.

However, the gap of such a nonlinear PC can be actively tuned by the input power, again leading to optical hysteresis and bistability. The authors found that the transmission associated with a zero- $\bar{n}$  gap exhibits a bistable characteristic that is relatively insensitive to incident angles, in contrast to the behavior of a usual Bragg gap. Such an incident-angle insensitivity of nonlinear responses can be traced back to the same insensitivity of linear optics in these systems.

Pan et al. generalized the two previous studies [48, 49] to more complicated cases [50], where the defect nonlinear layer can be either a LHM or a RHM, all LHM layers inside the PC are nonlinear, and even the nonlinear defect layer is a single-negative material. In all cases studied, they found that the optical bistability can still be obtained, exhibiting essentially the same unusual characteristics as in previous studies [48, 49].

In studying the optical properties of nonlinear LHM/RHM PCs, Hegde and Winful [51] noticed that inclusion of an intensity-dependent refractive index makes it possible to tune the stop band and thus switch the structure from a highly reflecting state to a totally transmitting state. As shown in Figure 16(A), the transmission through a 1D LHM/RHM PC at a frequency inside the zero- $\bar{n}$  gap is nearly zero in low-field regime, but becomes significantly enhanced when the incident field strength exceeds a critical value, and can reach 100% at a particular case [denoted by A in Figure 16(A)]. They found that such total transmission is due to the resonant excitation of a gap soliton state inside the nonlinear medium with field distribution depicted in Figure 16(B) [51]. The Bragg-gap soliton was first studied by Chen and Mills in 1987 [53], but here Hedge and Winful found the zero- $\bar{n}$  gap soliton exhibits a number of intriguing properties. In particular, it is an omnidirectional gap soliton which is insensitive to the propagating direction, and is also robust in the presence of disorder and loss [51].

### 4.3. Zero- $\bar{n}$ gaps in quasi-periodic and quasi-1D structures

Conventional Bragg gaps are formed by destructive interferences of EM waves in PCs, and clearly periodicity plays an

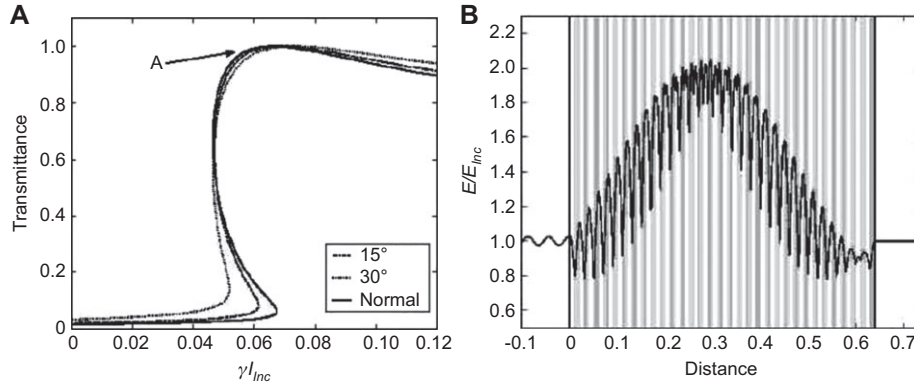


**Figure 16** (A) Hysteresis behavior of transmittance as a function of a defocusing  $\gamma I_{inc}$  for detuning to the left of the zero- $\bar{n}$  gap ( $f=3.51$  GHz,  $N=32$ ) for incident angles  $\theta=0^\circ$ ,  $15^\circ$ , and  $30^\circ$ . (B) Zero- $\bar{n}$  gap soliton: spatial distribution of the  $E$  field magnitude (normalized by  $E_{inc}$ ) when a defocusing  $\gamma I_{inc}=-0.064$  results in a near-unity transmittance ( $f=3.51$  GHz,  $N=32$ ) at normal incidence. Reproduced from Ref. [51] with the permission of Optical Society of America.

important role. However, the zero- $\bar{n}$  gap originates from the vanishing of refractive index and thus is insensitive to scaling and randomness. Therefore, it is natural to ask whether such an unusual gap can exist in certain *non-periodic* systems. Quasi-periodic structures are lying between periodic and random structures. Recently, several groups [54–57] theoretically studied the optical properties of a series of quasi-periodic layered structures formed by LHM and RHM slabs, arranged in Fibonacci or Thue–Morse sequences. These studies show that the zero- $\bar{n}$  gaps still survive in such non-periodic structures as long as the condition  $\bar{n}=0$  is satisfied. Many unusual properties discovered in periodic LHM-RHM PCs are still found in zero- $\bar{n}$  gaps of these non-periodic structures [54–57]. The existence of zero- $\bar{n}$  gaps in quasi-periodic PCs was experimentally verified by Zhang et al. in microstrip TL systems [40]. Recently, quasi-1D systems including comb-like [58, 59] and loop-like structures [60] were studied, and PBGs with essentially the same physics as the zero- $\bar{n}$  gap were discovered.

## 5. Ideas inspired by or related to the zero- $\bar{n}$ gap

After Li et al. introduced the concept of zero- $\bar{n}$  gap in 2003, many new ideas were inspired from this work, leading to interesting new physical predictions. Although these works were generally not directly on the zero- $\bar{n}$  gaps, they are highly correlated with the zero- $\bar{n}$  ideas. In this section, we briefly review these works and hope that further new ideas can be inspired.

### 5.1. Zero-phase ( $\phi_{eff}$ ) gap

The zero- $\bar{n}$  gaps were discovered in systems composed by *transparent* components, although their refraction indexes can be positive or negative. It is straightforward to ask if similar physics can happen in optical systems composed by *opaque* materials, such as epsilon-negative (ENG) media and mu-negative (MNG) media. In 2004, Jiang et al. [61] considered

a 1D PC formed by alternative stacking of ENG layers (with  $\varepsilon_1 < 0$ ,  $\mu_1 > 0$ , thickness  $d_1$ ) and MNG layers (with  $\varepsilon_2 > 0$ ,  $\mu_2 < 0$ , thickness  $d_2$ ). Based on the same mathematics, they found that the dispersion relation of the system is determined by

$$2 \cos(\kappa a) = 2 \cosh(k_1 d_1 - k_2 d_2) + \left( \frac{\eta_1 + \eta_2}{\eta_2 \eta_1} - 2 \right) \sinh(k_1 d_1) \sinh(k_2 d_2), \quad (14)$$

where  $k_i = \omega \sqrt{|\varepsilon_i \mu_i|} / c$  and  $\eta_i = \sqrt{|\mu_i / \varepsilon_i|}$ . Equation (14) is quite similar to Eq. (3), but an important difference is that the  $\cosh(x)$  function in Eq. (14) does not have to be bounded between  $-1$  and  $1$  like the  $\cos(x)$  function in Eq. (3). As a result, in most cases Eq. (14) does not have a real solution indicating that the system is intrinsically opaque. In 2003, Alu and Engheta showed that such systems can be *transparent* when material and geometrical parameters satisfy certain conditions, due to the interface resonance effects [62]. This discovery motivated people to ask the inverse question – under what condition should such system exhibit a PBG?

Jiang et al. [61] noticed that, when the *effective* phase accumulation (not the real phase since waves inside each layer are evanescent) across the unit cell is exactly zero, i.e.,

$$\phi_{eff} = k_1 d_1 - k_2 d_2 = 0, \quad (15)$$

$$\text{Eq. (14) becomes } 2 \cos(\kappa a) = 2 + \left( \frac{\eta_1 + \eta_2}{\eta_2 \eta_1} - 2 \right) [\sinh(k_1 d_1)]^2 \geq 2$$

indicating that a PBG must open here unless  $\eta_1 = \eta_2$  (impedance matching condition). The minus sign in front of  $k_2 d_2$  comes out because there is a  $\pi$  phase jump for the reflection at the ENG/MNG interface. The authors termed such a gap as the “zero effective phase (zero- $\phi_{eff}$ ) gap”, and proved that such a zero- $\phi_{eff}$  gap shared several interesting features as the zero- $\bar{n}$  gap, such as invariance against scaling and insensitive to disorder. Some years later, two groups independently pointed out that, in the long-wavelength limit (LWL), i.e.,  $k_1 d_1, k_2 d_2 \rightarrow 0$ , both zero- $\bar{n}$  and zero- $\phi_{eff}$  gaps are of the same

origin, with their upper/lower band edges determined by the  $\bar{\mu}=0$  and  $\bar{\varepsilon}=0$  conditions, respectively [63, 64]. This is not entirely surprising, since in the LWL the system behaves as an effective medium and it does not matter whether the unit cell is LHM/RHM or ENG/MNG. However, outside the LWL region, the zero- $\phi_{\text{eff}}$  gap behaves completely different from the zero- $\bar{n}$  gap, since these two gaps are, respectively, due to interactions between evanescent waves and propagating waves [63]. The existence of the zero- $\phi_{\text{eff}}$  was experimentally verified in 2008 [65].

## 5.2. Zero- $\varepsilon$ and zero- $\mu$ gaps and their interactions with the zero- $\bar{n}$ gap

Motivated by the discoveries of zero- $\bar{n}$  and zero- $\phi_{\text{eff}}$  gaps, people continued to search for other photonic gaps corresponding to vanishing of certain parameters. It is well known that a semi-finite medium with either  $\varepsilon=0$  or  $\mu=0$  is opaque for photons implying that a spectral gap opens. In a 1D PC formed by periodically stacking RHM (such as air) and dispersive LHM layers, the conditions  $\varepsilon(\omega)=0$  or  $\mu(\omega)=0$  could be satisfied for the dispersive LHM at certain frequencies. It is thus interesting to ask whether a zero- $\varepsilon$  or zero- $\mu$  gaps can open at these frequencies.

In a series of papers, Depine et al. [66, 67] demonstrated that such gaps do exist in 1D PCs, but only for oblique-transport cases. Extending Eq. (3) to off-normal situations assuming a fixed  $k_{\parallel}$ , the authors [66] found that the dispersions of photonic modes are determined by

$$2 \cos(\kappa a) = 2 \cos(k_{1z} d_1) \cos(k_{2z} d_2) - \left[ \frac{\sigma_2 k_{1z}}{\sigma_1 k_{2z}} + \frac{\sigma_1 k_{2z}}{\sigma_2 k_{1z}} \right] \sin(k_{1z} d_1) \sin(k_{2z} d_2), \quad (16)$$

where  $\sigma_j = \mu_j$  for TE polarization and  $\sigma_j = \varepsilon_j$  for TM polarization,  $k_{jz} = \sqrt{\varepsilon_j \mu_j (\omega/c)^2 - k_{\parallel}^2}$ . In general, the quantity inside the bracket (i.e., the impedance mismatch) is *singular* at the frequency where  $\mu_2(\omega) \rightarrow 0$  ( $\varepsilon_2(\omega) \rightarrow 0$ ) for the TE (TM) case. However, at normal incidence with  $k_{\parallel} = 0$ , we have simultaneously  $k_{2z} \rightarrow 0$  as  $\mu_2(\omega) \rightarrow 0$  (or  $\varepsilon_2(\omega) \rightarrow 0$ ), which compensates such a singularity, so that no gaps can be observed. Interestingly, away from the normal incidence,  $k_{2z}$  becomes a finite number which cannot compensate the singularity in  $\mu_2$  (or  $\varepsilon_2$ ). Thus, a spectral gap must open when  $k_{\parallel}$  exceeds a critical value, at the frequency corresponding to zero- $\mu$  (zero- $\varepsilon$ ) for TE (TM) polarization. Shown in Figure 17 are the dispersion diagrams of the 1D PC studied previously by Li et al. [36], but calculated for *oblique incidence cases* in different polarizations [66]. Indeed, at oblique incidences, a zero- $\mu$  gap is developed for TE polarization while a zero- $\varepsilon$  gap is developed for TM polarization.

Similar to the zero- $\bar{n}$  and zero- $\phi_{\text{eff}}$  gaps, such zero- $\varepsilon$  and zero- $\mu$  gaps are also due to the intrinsic properties of constitutive materials rather than geometrical structures. Therefore, these non-Bragg gaps share lots of common characteristics, such as insensitivities to length scaling and weak disorder.

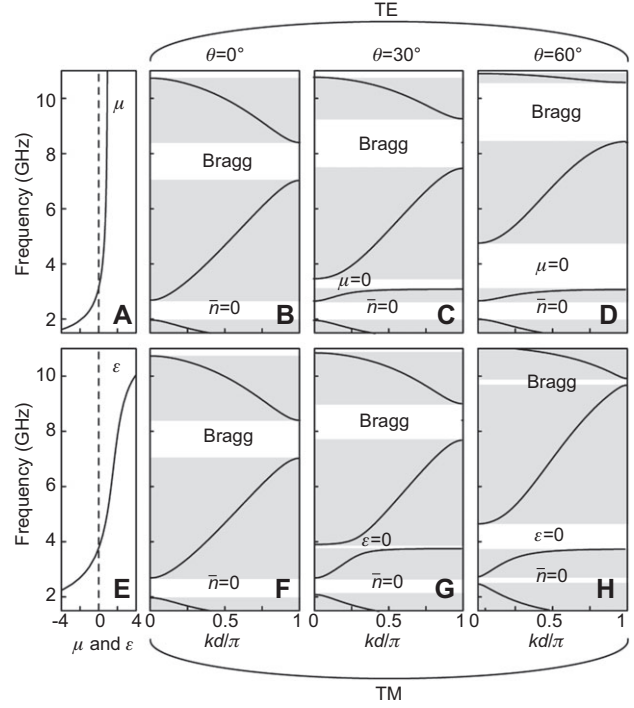


**Figure 17** Band structures for TE and TM polarizations and different angles of incidence corresponding to a periodic stack with alternating air layers ( $\mu_1 = \varepsilon_1 = 1$ ,  $d_1 = 12$  mm) and MTM layers with  $\mu_2$  and  $\varepsilon_2$  given by Eq. (13) and  $d_2 = 6$  mm. The left column shows the frequency dispersions of the constitutive parameters for layer 2. Reproduced from Ref. [66] with the permission of Elsevier.

More intriguingly, the zero- $\varepsilon$  and zero- $\mu$  gaps are solely determined by the properties of a *single* layer, which further differentiate themselves from the zero- $\bar{n}$  and zero- $\phi_{\text{eff}}$  gaps. Therefore, if we change the volume ratio  $d_1/d_2$  between two constitutive layers, the position of the zero- $\bar{n}$  gap can be tuned significantly while those of the zero- $\varepsilon$  and zero- $\mu$  gaps remain unchanged. The same group of authors then studied the interesting interplays between these two non-Bragg gaps [67], by carefully adjusting the volume ratio  $d_1/d_2$ . Singh et al. further pointed out that such zero- $\varepsilon$  and zero- $\mu$  gaps can exist in any 1D PCs, not necessarily only in RHM/RHM superlattices, and studied the properties of defect modes in such band gaps [68].

In 2009, Reyes-Gómez et al. [69] proposed a different but rather inspiring interpretation for such zero- $\varepsilon$  and zero- $\mu$  gaps. Noticing that  $\varepsilon=0$  ( $\mu=0$ ) corresponds to (bulk) plasmon polariton (PP) excitation of the dispersive medium (layer 2), the authors argued that such gaps arise from the interactions between propagating modes and bulk PPs. Since the PPs are longitudinal excitations, they can be excited only when there is an E (or H) field component along z direction, which explained why such gaps can only be seen at off-normal incidences. Through adjusting the volume ratio, the authors can tune the zero- $\varepsilon$  (zero- $\mu$ ) gaps to appear inside the zero- $\bar{n}$  gap, and found that the interactions between propagating waves and PPs are significantly weakened in such a case. The same

group further studied such gaps and their interplays with the zero- $\bar{n}$  gap in 1D systems with quasi-periodicity [70] and anisotropy [71].

### 5.3. Complete band gaps

One of the key motivations in PC studies is to find a material possessing a complete PBG, inside which no EM wave can propagate along *any* direction. Since a Bragg gap is formed by destructive EM wave interferences, one naturally expects that a complete PBG needs a structure with periodic modulations along all three directions. A 1D PC formed by alternative stacking of ordinary material slabs can never exhibit a complete PBG, since there is no mechanism to suppress the waveguiding propagations inside the layers formed by optically dense medium [72]. Since the zero- $\bar{n}$  gap was found to exhibit omnidirectional reflectivity (see Figure 3), it is natural to ask whether it is a complete PBG or not. We emphasize that the omnidirectional reflectivity does not necessarily imply a complete PBG, since the latter is more strict, requiring that no mode can exist for any  $k_{\parallel}$  values including the cases of  $k_{\parallel} > \omega/c$ .

Shadrivov et al. studied the problem in detail [73]. By thoroughly examining the Bloch equations for two polarizations [i.e., Eq. (16)], they found that a complete PBG could indeed be formed in 1D PCs containing LHM layers, when the material and geometrical parameters satisfy certain strict conditions. In a 1D PC, a waveguide mode always exists when the phase matching condition  $2\phi_{\text{prop}} + 2\phi_{\text{Ref1}} = 2m\pi$  is satisfied, where  $\phi_{\text{prop}}$  is the propagating phase accumulation and  $\phi_{\text{Ref1}}$  the reflection phase at an interface between two adjacent layers. The authors found that, by choosing LHMs with appropriate parameters, it is possible to make the phase-matching condition unsatisfied for all  $k_{\parallel}$  values. Combining this condition with the Bragg gap condition, the authors successfully obtained the parameter regions where a complete PBG exists in a 1D PC. They also visualized the complete PBG effect by numerically studying the radiation pattern of a point source inside a carefully designed 1D PC possessing a complete PBG. Figure 18 clearly shows that EM wave propagations along all directions are suppressed inside such a 1D PC. Later, Sun et al. [74] studied the 1D PCs containing *anisotropic* LHMs, and found that the anisotropy offers expanded freedoms to realize the complete PBG effect. Interestingly, they found that a complete PBG requires an  $m=1$  Bragg gap rather than the zero- $\bar{n}$  gap [74].

## 6. Extensions to higher dimensions: Zero-index metamaterials and Dirac-cone physics

The zero- $\bar{n}$  systems we discussed so far are 1D systems. If we want to extend the idea to higher dimensions, we note that the optical path length is zero when a wave goes through a stack of zero- $\bar{n}$  material. The zero optical path length is the essence of the physics underlying the properties of these materials. Before we proceed, we remark that if we restrict our discussion to 1D, the zero- $\bar{n}$  material is related to the complementary

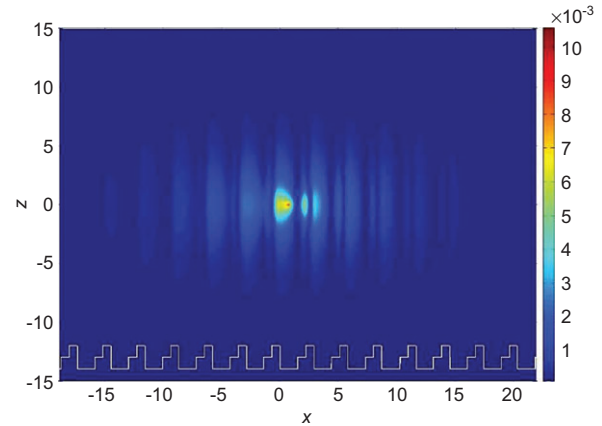


**Figure 18** Computed radiation pattern of a point source placed inside a 1D PC possessing a complete band gap. Reproduced from Ref. [73] with the permission of American Physics Society.

medium proposed by Pendry and Ramakrishna [75]. A subset of complementary media can be regarded as a zero- $\bar{n}$  material that is impedance matched and in this case, the wave goes through the media with unity transmittance and zero phase change. In 1D, zero optical path length can be achieved if the average refractive index along the propagation direction is zero, but in 2D or 3D, it is difficult to require the average  $n$  along all directions to be zero. We can instead require the *effective* refractive index to be zero. As we are dealing with composite materials, a zero refractive index should be understood within the context of an effective medium or “homogenization”. A material with effectively zero- $n$  can have either zero effective  $\epsilon$ , zero effective  $\mu$ , or both zero effective  $\epsilon$  and zero effective  $\mu$  simultaneously.

Snell’s law tells us that only the normal incident wave can go through a zero index material (ZIM), while other oblique angle waves are totally reflected. In addition, there is no phase variance in the wave transport process. This leads to many peculiar properties, such as the tailoring of the radiation phase pattern [76], collimating light [77, 78], tunneling of waves through arbitrary subwavelength channels and bends [79–84], and cloaking objects inside a channel with specific boundary conditions [85–88]. In the following part, we will illustrate some of these properties.

The zero phase change property of a ZIM can be used to tailor the wave front by configuring the interface [76, 77]. When a normal incident plane wave illuminates the flat left entrance face of a slab of epsilon-near-zero material (one realization of ZIMs) with a concave exit face, because of the identical phase in the exit face, EM field is focused at the center of curvature of the output interface [76]. A ZIM with a flat interface can be used to collimate light. Figure 19 shows the FDTD simulation results when a line source is placed at the center of a ZIM slab with  $\epsilon=\mu=0$ . We see that the radiation fields propagate through the slab with a direction orthogonal to the interface of the slab (shown in Figure 19) [77] as required by Snell’s law. The cylindrical wave generated by the line source is converted into a wave with a planar wave front.

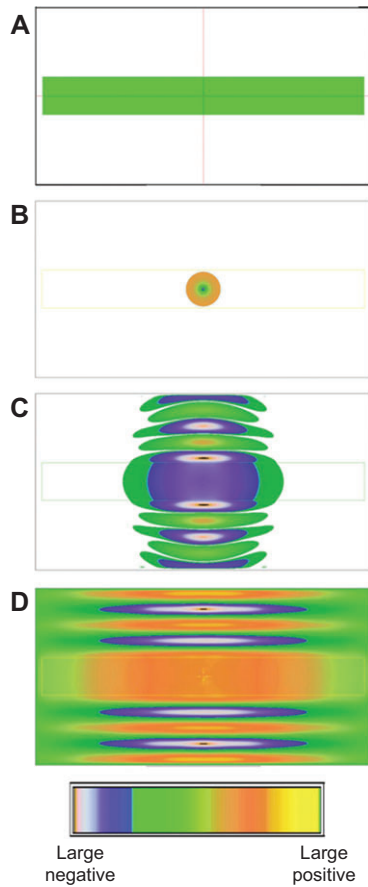


**Figure 19** The instant electric field distribution at different time intervals calculated by FDTD simulation, which is produced by a line source located in the middle of a slab filled with matched zero-index Drude medium. (A)  $t=0$ , (B)  $t=200\Delta t$ , (C)  $t=800\Delta t$ , and (D)  $t=2200\Delta t$ . Reproduced from Ref. [77] with the permission of American Physical Society.

Another special property of ZIM is that EM waves can be “squeezed” and tunneled through very narrow and arbitrary-shaped channels as long as the total volume is small and such effect has been demonstrated using epsilon-near-zero materials [79–84]. The incoming plane wave can be replicated at the output interface. The tunneling phenomenon has been realized by sophisticated experiments using complementary split ring resonators at the microwave frequency [82].

Recently, the method of transformation optics has enabled the design of many intriguing wave manipulation devices such as invisibility cloaks [24–27], EM field concentrators [89], superscatterer [90], field rotators [91] and illusion optics [28]. ZIMs can also be used to block waves with an arbitrary small inclusion (super-reflection) or conceal objects completely (cloaking) under certain conditions [85]. While ZIMs can perform cloaking under restricted conditions inside a waveguide, they are less complex in structure than materials designed by transformation optics. The “super-reflection” device can be realized by a  $\mu=0$  ( $\epsilon=0$ ) MTM with a perfect electric (magnetic) conductor inclusion of arbitrary shape and size for a TE (TM) incident wave (Figure 20A). In

contrast, a  $\mu=0$  ( $\epsilon=0$ ) MTM with a perfect magnetic (electric) conductor inclusion for a TE (TM) incident wave can be used to conceal objects of arbitrary shape (Figure 20B). The underlying physics here are again determined by the fact that in steady state, the EM fields in the ZIM material are static without phase variation in space. The effects are numerically demonstrated by full wave simulations (see Figure 20). In addition, super-reflection and cloaking effect can also be achieved through tuning resonant cavities imbedded in ZIMs [86, 87].

In practice, the ZIMs can be made by MTMs using some specific resonant metallic inclusions, which can in principle operate at any frequency regime. However, at IR or optical frequencies, the material loss should be taken into account and dissipation will compromise the use of resonant metallic structure to realize ZIMs. In addition, many ZIMs considered previously are “single-zero” material [76, 78–85, 87, 88], meaning that only one of the material parameters is zero at a specific frequency (either  $\epsilon=0$  or  $\mu=0$  but not both). This is quite natural as it would be quite challenging to obtain  $\epsilon=\mu=0$  simultaneously using metallic resonators. However, for a single-zero material, the impedance mismatch is huge and the incident wave will encounter reflection when the aperture of the waveguide is larger than wavelength [76, 88]. It would be highly desirable if one could get a ZIM without using metallic inclusions (avoid material loss) and  $\epsilon_{eff}=\mu_{eff}=0$  simultaneously. We note that the group velocity is zero for a single-zero material which can be undesirable for many applications, while a material with  $\epsilon_{eff}=\mu_{eff}=0$  possesses a finite group velocity. It turns out that a certain class of 2D dielectric PCs that possess

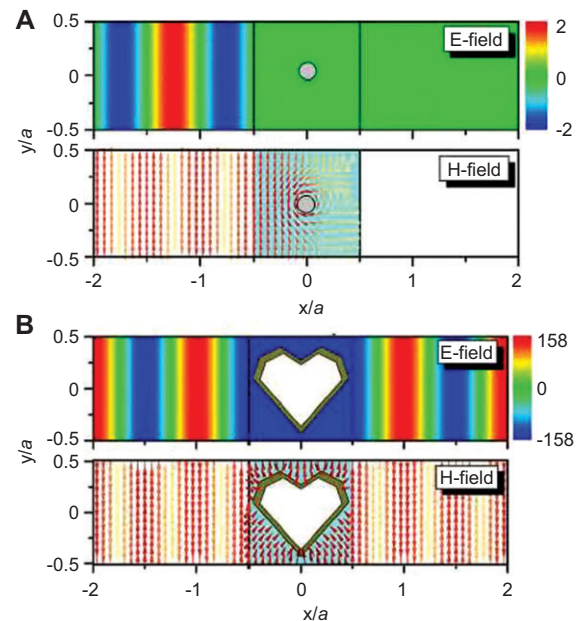


**Figure 20** The electric field ( $E_z$ ) and magnetic fields ( $H_x, H_y$ ) distributions with perfect electric conductor (A) and perfect magnetic conductor (B) objects imbedded in the zero-index material. Reproduced from Ref. [85] with the permission of American Institute of Physics.

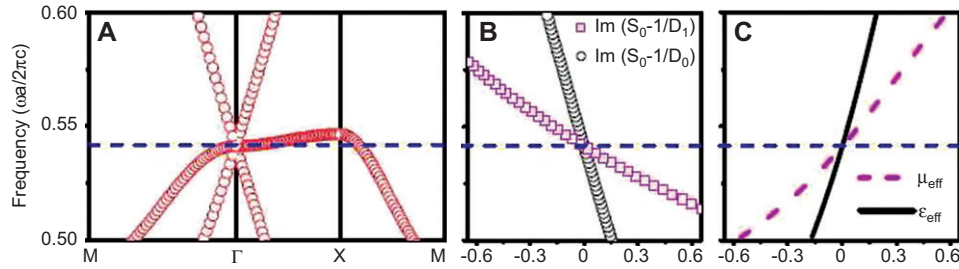


**Figure 21** (A) Band structure of a 2D PC consisting of dielectric cylinders with radius  $R=0.2a$ , relative permittivity  $\epsilon=12.5$  and permeability  $\mu=1$ . (B) Value of imaginary part of the scattering coefficients  $S_0-1/D_0$  (black open circles) and  $S_0-1/D_1$  (pink open squares) as functions of frequency for the PC with band structure shown in (A). (C) The effective permittivity  $\epsilon_{eff}$  (black solid line) and permeability  $\mu_{eff}$  (pink dashed line) as functions of frequency for the 2D PC.

Dirac-cone like dispersions at the  $\Gamma$  point ( $k=0$ ) can be mapped to double-zero ( $\epsilon_{eff}=\mu_{eff}=0$ ) material [92]. If such 2D dielectric PCs can be fabricated using nanofabrication techniques [93], we can realize ZIMs at optical frequencies with low-loss and good impedance matching.

In a dispersive homogenous system with  $\epsilon=\mu=0$ , it is straightforward to show that the dispersion at  $k=0$  is linear and conical dispersion (Dirac cone) exists naturally [94]. However, the converse is not necessarily true as will be explained below. The Dirac cone dispersions can be found in the electronic band structure in graphene [95–97], and in the band structure of classical wave systems such as photonic [98] or phononic crystals [99] with a honeycomb or triangular lattice. The possibility of *simulating* relativistic particle behaviors in condensed-matter or classical wave experiments, such as quantum hall effect [96], the Klein tunneling [97] and Zitterbewegung effect [99], has attracted much attention. The aforementioned Dirac cones in graphene [95–97] and photonic/phononic crystals [98, 99] exist at the Brillouin zone boundary. If we want to use a PC to emulate a  $\epsilon_{eff}=\mu_{eff}=0$  system, we need to apply effective medium theory but effective medium theories cannot be applied to  $k$ -points at the zone boundary. We need to find Dirac cone dispersions at the zone center.

The Dirac cones at the K point (zone boundary) in PCs [98] with triangular or honeycomb lattices are the consequences of the lattice symmetry. However, lattice symmetry alone can

only give parabolic dispersion at the  $\Gamma$  point. We can employ accidental degeneracy to get linear band dispersions at the  $\Gamma$  point, which is needed for Dirac cones. Figure 21 shows an example of how this can be achieved. The band structure of a 2D PC consisting of a square lattice of dielectric cylinders for the TM polarization (with E field along the cylinder axis) is shown in Figure 21(A) [92]. Here, the radius and relative permittivity of the cylinders are set at  $R=0.2a$  ( $a$  is the lattice constant) and  $\epsilon=12.5$ . There is a triply-degeneracy at the  $\Gamma$  point, composing of two linear bands and another quadratic band intersecting at the same frequency [see Figure 21(A)]. The two linear bands generate a Dirac cone. We show the field patterns of the eigenmodes near the Dirac point with a small  $k$  along  $\Gamma X$  direction in Figure 22. Figures 22(A) and (B) show that the linear bands are linear combinations of the monopole and transverse dipole with its magnetic field polarized perpendicular to the wave vector, while the flat band corresponds to quasi-longitudinal dipole with its magnetic field polarized parallel to the wave vector [see Figure 22(C)]. In general, the eigenfrequency of the monopole is not equal to that of the dipole, and three-fold degeneracy at the  $\Gamma$  point is “accidental” in the sense that it is not a consequence of lattice symmetry but rather a consequence of specifically chosen structural parameters. In the present PC system in which the bands originate from monopole and dipole excitations, the recipe to get the accidental degeneracy can be formulated in mathematical terms using multiple scattering theory. It can

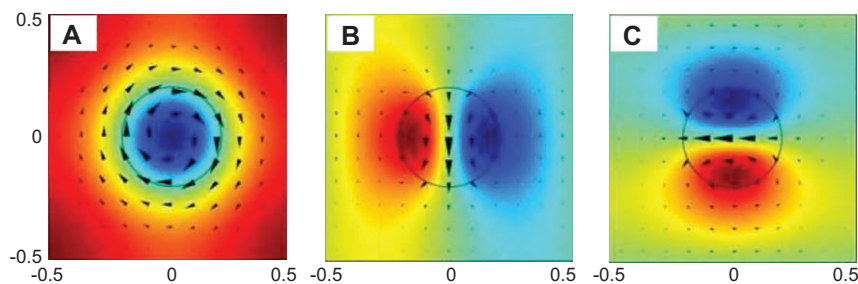


**Figure 22** Field patterns of the eigenmodes near the Dirac point with a very small  $k$  along  $\Gamma X$  direction. The color patterns show the  $E_z$  fields and the vector fields show  $\vec{H}$  fields. (A) The real part of  $E_z$  and the imaginary part of  $\vec{H}$  at the frequency  $0.527c/a$ , (B) The imaginary part of the  $E_z$  and the real part of  $\vec{H}$  at the frequency  $0.527c/a$ , (C) The real part of  $E_z$  and the imaginary part of  $\vec{H}$  at the frequency  $0.541c/a$ .

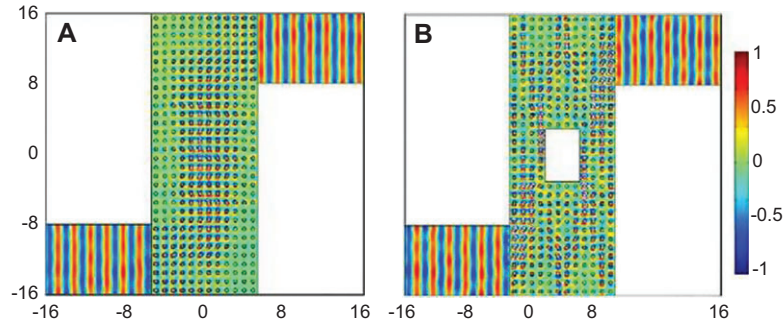


**Figure 23** Numerical simulated electric field ( $E_z$ ) patterns in the 90 degree bending channel. (A)  $E_z$  distribution if the 90 degree bending channel is filled with the designed 2D PC. (B)  $E_z$  distribution if the 90 degree bending channel is filled with PCs with an embedded PMC object. The incident wave is plane wave and the boundary conditions of the channel are PMC. The working frequency is  $0.541c/a$ .

be shown (see Ref. 92) that if  $S_0=1/D_0=1/D_{\pm 1}$ , the dispersion near  $k=0$  has a triply-degenerate state. Here,  $S_0$  is a lattice sum which depends on  $k$  and  $\omega$ , while  $D_0$  and  $D_{\pm 1}$  are the scattering matrix coefficients of the cylinder for monopole and dipole (see Ref. 92 for mathematical details). Among the three solutions, one has a quadratic dispersion while the other two solutions have a leading linear term giving rise to linear bands with opposite and non-zero group velocities  $\pm v_g$  which is the same for all directions. For a given value of permittivity and a given lattice constant, the condition  $S_0=1/D_0=1/D_{\pm 1}$  can be achieved by choosing a specific rod radius. To show that this condition is indeed satisfied in the PC that bears a Dirac cone at  $k=0$ , we plot in Figure 21(B) the values of the imaginary part of  $S_0-1/D_0$  and  $S_0-1/D_1$  ( $S_0-1/D_0$  and  $S_0-1/D_1$  are purely imaginary numbers) as functions of frequency for the parameters shown in Figure 21(A). The condition  $S_0=1/D_0=1/D_{\pm 1}$  is indeed satisfied at the Dirac point frequency ( $f=0.541c/a$ ).

Effective medium theory [100] is then applied to calculate the effective medium parameters for this PC, and the effective permittivity ( $\epsilon_{\text{eff}}$ ) and permeability ( $\mu_{\text{eff}}$ ) as functions of frequency are shown in Figure 21(C). We see that  $\epsilon_{\text{eff}}$  and  $\mu_{\text{eff}}$  indeed intersect at zero at the Dirac frequency. In addition, Figures 21(B) and 21(C) show that the frequency at which  $\epsilon_{\text{eff}}=\mu_{\text{eff}}=0$  is precisely the accidental degeneracy frequency defined by  $S_0=1/D_0=1/D_{\pm 1}$ . Since  $\epsilon_{\text{eff}}$  and  $\mu_{\text{eff}}$  approach zero simultaneously and linearly, the effective impedance of such

a PC is a finite constant and the group velocity is also non-zero there. We now have a design recipe for PCs that behave like a ZIM with a finite group velocity which does not require any metallic inclusions.

As the PC is effectively  $\epsilon_{\text{eff}}=\mu_{\text{eff}}=0$  at the Dirac point, it should behave like a ZIM at frequencies near the Dirac point. For example, Figure 23(A) shows that waves can go around a 90 degree waveguide filled with the 2D PC and exit in the upper right channel with little distortion, as predicted previously [79]. The boundary conditions of the channels are perfect magnetic conductors (PMCs). Previous studies showed that an embedded object with PMC boundaries is “invisible” inside a channel filled with a homogeneous zero- $n$  material [85]. Figure 23(B) shows that if an object with PMC boundary conditions is inserted into the channel filled with our designed PC, the wave just passes through the channel as if the obstacle were not there, manifesting the cloaking effects expected if the filling material has a zero effective index.

The “wave front transformer” effect of ZIM can also be demonstrated. As we have mentioned above [76], a homogeneous ZIM can focus wave with a concave exit interface profile as demonstrated numerically in Figure 24(A). A plane wave is incident from the left, and as there is no phase change across the medium, the phase is the same on the concave surface, leading to the formation of a focal point on the right side of the lens. In Figure 24(B), the homogeneous medium is

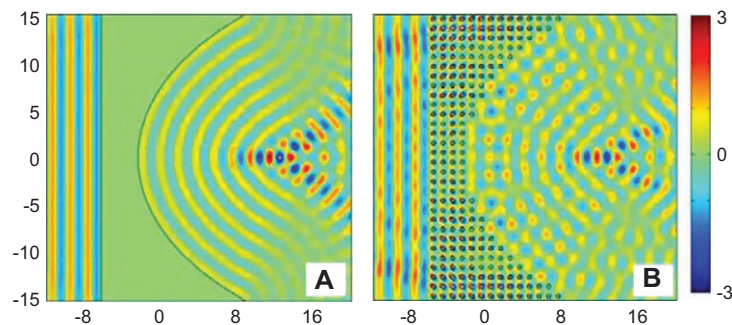


**Figure 24** Simulated field distributions when a lens [with a flat (concave) interface on the left (right)] formed by (A) a homogeneous  $\epsilon=\mu=0$  medium and (B) the designed 2D PC are illuminated by a plane wave coming from the left. The working frequency is  $0.541c/a$ .

replaced by a 2D PC with the configuration and band structure shown in Figure 21(A). At or near the Dirac point frequency, the field pattern is similar to the homogeneous case and in particular, the wave is focused to the same position on the right-hand side of the PC. We note that this phenomenon has been verified experimentally in the microwave regime with PC constructed using alumina rods [92].

## 7. Conclusions

In this paper, we briefly reviewed the fundamental physics and latest developments in research field of zero- $\bar{n}$  gap. Besides introducing the basic concept, key properties, experimental verifications, and potential applications of such an unusual gap, we also tried to include several new ideas inspired from the zero- $\bar{n}$  research. These works, including the zero- $\phi_{\text{eff}}$  gap, the zero- $\epsilon$  and zero- $\mu$  gaps, the complete band gap, and the zero-index materials, may not have direct relations with the zero- $\bar{n}$  research. However, they are strongly correlated and share a lot of common characteristics with the zero- $\bar{n}$  research. We hope that presenting them together in a concise and coherent way may stimulate further research works, and we look forward to new ideas inspired from this review.

## Acknowledgements

This work was supported by NSFC (Nos. 60990321, 11174055), MOE of China (No. B06011), Program of Shanghai Subject Chief Scientist (12XD1400700), and Hong Kong RGC GRF grant 600311.

## References

- [1] Joannopoulos JD, Villeneuve PR, Fan S. Photonic crystal: putting a new twist on light. *Nature* 1997;386:143–9.
- [2] Yablonovitch E. Inhibited spontaneous emission in solid-state physics and electronics. *Phys Rev Lett* 1987;58:2059–62.
- [3] Soukoulis CM. *Photonic Band Gaps and Localization*. New York: Plenum; 1993.
- [4] Veselago VG. The electrodynamics of substances with simultaneously negative value of  $\epsilon$  and  $\mu$ . *Sov Phys Usp* 1968;10:509–14.
- [5] Pendry JB, Holden AJ, Stewart WJ, Youngs I. Extremely low frequency plasmons in metallic mesostructures. *Phys Rev Lett* 1996;76:4773–6.
- [6] Pendry JB, Holden AJ, Robbins DJ, Stewart WJ. Magnetism from conductors and enhanced nonlinear phenomena. *IEEE Trans Microwave Theory Tech* 1999;47:2075–84.
- [7] Smith DR, Padilla WJ, View DC, Nemat-Nasser SC, Schultz S. Composite medium with simultaneously negative permeability and permittivity. *Phys Rev Lett* 2000;84:4184–7.
- [8] Shelby RA, Smith DR, Schultz S. Experimental verification of a negative index of refraction. *Science* 2001;292:77–9.
- [9] Smith DR, Pendry JB, Wiltshire MCK. Metamaterials and negative refractive index. *Science* 2004;305:788–92.
- [10] Lodahl P, Driel AF, Nikolaev IS, Irman A, Overgaag K, Vanmaekelbergh D, Vos WL. Controlling the dynamics of spontaneous emission from quantum dots by photonic crystals. *Nature* 2004;430:654–7.
- [11] Fink Y, Winn JN, Fan S, Chen C, Michel J, Joannopoulos JD, Thomas EL. A dielectric omnidirectional reflector. *Science* 1998;282:1679–82.
- [12] Hart SD, Maskaly GR, Temelkuran B, Prideaux PH, Joannopoulos JD, Fink Y. External reflection from omnidirectional dielectric mirror fibers. *Science* 2002;296:510–3.
- [13] Li ZY, Zhang ZQ. Fragility of photonic band gaps in inverse-opal photonic crystals. *Phys Rev B* 2000;62:1516–9.
- [14] Sigalas MM, Soukoulis CM, Chan CT, Biswas R, Ho KM. Effect of disorder on photonic band gaps. *Phys Rev B* 1999;59:12767–70.
- [15] Asatryan AA, Robinson PA, Botten LC, McPhedran RC, Nicorovici NA, Sterke CM. Effects of geometric and refractive index disorder on wave propagation in two-dimensional photonic crystals. *Phys Rev E* 2000;62:5711–20.
- [16] Fan S, Villeneuve PR, Joannopoulos JD. Theoretical investigation of fabrication-related disorder on the properties of photonic crystals. *J Appl Phys* 1995;78:1415–8.
- [17] Smith DR, Schultz S, Markos P, Soukoulis CM. Determination of effective permittivity and permeability of metamaterials from reflection and transmission coefficients. *Phys Rev B* 2002;65:195104.
- [18] Pendry JB. Negative refraction. *Contemp Phys* 2004;45:191–202.
- [19] Ramakrishna SA. Physics of negative refractive index materials. *Rep Prog Phys* 2005;68:449–521.
- [20] Pendry JB. Negative refraction makes a perfect lens. *Phys Rev Lett* 2000;85:3966–9.
- [21] Garcia N, Nieto-Vesperinas M. Left-handed materials do not make a perfect lens. *Phys Rev Lett* 2002;88:207403.
- [22] Grbic A, Eleftheriades GV. Overcoming the diffraction limit with a planar left-handed transmission-line lens. *Phys Rev Lett* 2004;92:117403.
- [23] Parimi PV, Lu WT, Vodo P, Sridhar S. Imaging by flat lens using negative refraction. *Nature* 2003;426:404.
- [24] Pendry JB, Schurig D, Smith DR. Controlling electromagnetic fields. *Science* 2006;312:1780–2.
- [25] Leonhardt U. Optical conformal mapping. *Science* 2006;312:1777–80.
- [26] Schurig D, Mock JJ, Justice BJ, Cummer SA, Pendry JB, Starr AF, Smith DR. Metamaterial electromagnetic cloak at microwave frequencies. *Science* 2006;314:977–80.
- [27] Li J, Pendry JB. Hiding under the carpet: a new strategy for cloaking. *Phys Rev Lett* 2008;101:203901.
- [28] Lai Y, Ng J, Chen HY, Han DZ, Xiao JJ, Zhang ZQ, Chan CT. Illusion optics: the optical transformation of an object into another object. *Phys Rev Lett* 2009;102:253902.
- [29] Houck AA, Brock JB, Chuang IL. Experimental observations of a left-handed material that obeys Snell's law. *Phys Rev Lett* 2003;90:137401.
- [30] Chen JB, Wang Y, Jia BH, Geng T, Li XP, Feng L, Qian W, Liang BM, Zhang XX, Gu M, Zhuang SL. Observation of the inverse Doppler effect in negative-index materials at optical frequencies. *Nature Photon* 2011;5:239–45.
- [31] Xi S, Chen HS, Jiang T, Ran LX, Huangfu JT, Wu BI, Kong JA, Chen M. Experimental verification of reversed cherenkov radiation in left-handed metamaterial. *Phys Rev Lett* 2009;103:194801.
- [32] Landau L, Lifschitz EM. *Electrodynamics of Continuous Media*. New York: Elsevier; 1984.
- [33] Foteinopoulou S, Soukoulis CM. Negative refraction and left-handed behavior in two-dimensional photonic crystals. *Phys Rev B* 2003;67:235107.

- [34] Foteinopoulou S, Economou EN, Soukoulis CM. Refraction in media with a negative refractive index. *Phys Rev Lett* 2003;90:107402.
- [35] Luo CY, Johnson SG, Joannopoulos JD, Pendry JB. All-angle negative refraction without negative effective index. *Phys Rev B* 2002;65:201104(R).
- [36] Li J, Zhou L, Chan CT, Sheng P. Photonic band gap from a stack of positive and negative index materials. *Phys Rev Lett* 2003;90:083901.
- [37] Jiang HT, Chen H, Li HQ, Zhang YW, Zhu SY. Omnidirectional gap and defect mode of one-dimensional photonic crystals containing negative-index materials. *Appl Phys Lett* 2003;83:5386–8.
- [38] Yuan Y, Ran LX, Huangfu JT, Chen HS, Shen LF, Kong JA. Experimental verification of zero order bandgap in a layered stack of left-handed and right-handed materials. *Opt Express* 2006;14:2220–7.
- [39] Chen H, Ran L, Huangfu JT, Zhang X, Chen K, Grzegorzczuk TM, Kong JA. Negative refraction of a combined double S-shaped metamaterial. *Appl Phys Lett* 2005;86:151909.
- [40] Zhang LW, Zhang YW, He L, Wang ZG, Li HQ, Chen H. Zero- $\bar{n}$  gaps of photonic crystals consisting of positive and negative index materials in microstrip transmission lines. *J Phys D: Appl Phys* 2007;40:2579–83.
- [41] Kocaman S, Chatterjee R, Panoiu NC, McMillan JF, Yu MB, Osgood RM, Kwong DL, Wong CW. Observation of Zeroth-Order band gaps in negative-refraction photonic crystal superlattices at near-infrared frequencies. *Phys Rev Lett* 2009;102:203905.
- [42] Chatterjee R, Panoiu N, Liu K, Dios Z, Yu M, Doan M, Kaufman L, Osgood R, Wong CW. Achieving subdiffraction imaging through bound surface states in negative refraction photonic crystals in the near-infrared range. *Phys Rev Lett* 2008;100:187401.
- [43] Panoiu NC, Osgood RM, Jr, Zhang S, Brueck SRJ. Zero- $\bar{n}$  bandgap in photonic crystal superlattices. *J Opt Soc Am B* 2006;23:506–13.
- [44] Mocella V, Cabrini S, Chang ASP, Dardano P, Moretti L, Rendina I, Olynick D, Harteneck B, Dhuey S. Self-Collimation of Light over Millimeter-Scale Distance in a Quasi-Zero-Average-Index Metamaterial. *Phys Rev Lett* 2009;102:133902.
- [45] Shadrivov IV, Sukhorukov AA, Kivshar YS. Beam shaping by a periodic structure with negative refraction. *Appl Phys Lett* 2003;82:3820–2.
- [46] Davoyan AR, Shadrivov IV, Sukhorukov AA, Kivshar YS. Bloch oscillations in chirped layered structures with metamaterials. *Opt Express* 2008;16:3299–304.
- [47] Davoyan AR, Sukhorukov AA, Shadrivov IV, Kivshar YS. Beam oscillations and curling in chirped periodic structures with metamaterials. *Phys Rev A* 2009;79:013820.
- [48] Feise MW, Shadrivov IV, Kivshar YS. Tunable transmission and bistability in left-handed band-gap structures. *Appl Phys Lett* 2004;85:1451–3.
- [49] Hegde RS, Winful HG. Optical bistability in periodic nonlinear structures containing left handed materials. *Microw Opt Techn Lett* 2005;46:528–30.
- [50] Pan T, Tang CJ, Gao L, Li ZY. Optical bistability of nonlinear multilayered structure containing left-handed materials. *Phys Lett A* 2005;337:473–9.
- [51] Hegde RS, Winful HG. Zero- $n$  gap soliton. *Opt Lett* 2005;30:1852–4.
- [52] Winful HG, Marburger JH, Garmire E. Theory of bistability in nonlinear distributed feedback structures. *Appl Phys Lett* 1979;35:379–81.
- [53] Chen W, Mills DL. Gap solitons and the nonlinear optical response of superlattices. *Phys Rev Lett* 1987;58:160–3.
- [54] Li J, Zhao DG, Liu ZY. Quasiperiodic stacking of positive and negative refractive index materials. *Phys Lett A* 2004;332:461–8.
- [55] Zhang HY, Zhang YP, Shang TY, Zheng Y, Ren GJ, Wang P, Yao JQ. Omnidirectional zero- $\bar{n}$  gap in symmetrical Fibonacci sequences composed of positive and negative refractive index materials. *Eur Phys J B* 2006;52:37–40.
- [56] He H, Zhang WY. Transmission spectra in symmetrical Fibonacci superlattices composed of positive and negative refractive index materials. *Phys Lett A* 2006;351:198–204.
- [57] Monsoriu JA, Depine RA, Silvestre E. Non-Bragg band gaps in 1D metamaterial aperiodic multilayers. *J Eur Opt Soc Rapid* 2007;2:07002.
- [58] Weng Y, Wang ZG, Chen H. Band structure of comb-like photonic crystals containing meta-materials. *Opt Commun* 2007;277:80–3.
- [59] Zhang LW, Wang ZG, Chen H, Li HQ, Zhang YW. Experimental study of quasi-one-dimensional comb-like photonic crystals containing left-handed material. *Opt Commun* 2008;281:3681–5.
- [60] Tan W, Wang ZG, Chen H. Photonic band gap of loop structure containing negative-index materials. *Phys Rev E* 2008;77:026603.
- [61] Jiang HT, Chen H, Li HQ, Zhang YW, Zi J, Zhu SY. Properties of one-dimensional photonic crystals containing single-negative materials. *Phys Rev E* 2004;69:066607.
- [62] Alú A, Engheta N. Pairing an Epsilon-Negative Slab With a Mu-Negative Slab: Resonance, Tunneling and Transparency. *IEEE Trans Antennas Propag* 2003;51:2558–71.
- [63] Weng Y, Wang ZG, Chen H. Band structures of one-dimensional subwavelength photonic crystals containing metamaterials. *Phys Rev E* 2007;75:046601.
- [64] Gao L, Tang CJ, Wang SM. Photonic band gap from a stack of single-negative materials. *J Magn Magn Mater* 2006;301:371–7.
- [65] Zhang LW, Zhang YW, He L, Li HQ, Chen H. Experimental investigation on zero- $\phi_{\text{eff}}$  gap of photonic crystals containing single-negative materials. *Eur Phys J B* 2008;62:1–6.
- [66] Depine RA, Martínez-Ricci ML, Monsoriu JA, Silvestre E, Andrés P. Zero permeability and zero permittivity band gaps in 1D metamaterial photonic crystals. *Phys Lett A* 2007;364:352–5.
- [67] Monsoriu JA, Depine RA, Martínez-Ricci ML, Silvestre E. Interaction between non-Bragg band gaps in 1D metamaterial photonic crystals. *Opt Express* 2006;14:12958–67.
- [68] Singh SK, Pandey JP, Thapa KB, Ojha SP. Some new band gaps and defect modes of 1D photonic crystals composed of metamaterials. *Solid State Commun* 2007;143:217–22.
- [69] Reyes-Gómez E, Mogilevtsev D, Cavalcanti SB, Carvalho CAA, Oliveira LE. Plasmon polaritons in photonic superlattices containing a left-handed material. *Europhys Lett* 2009;88:24002.
- [70] Reyes-Gómez E, Raigoza N, Cavalcanti SB, Carvalho CAA, Oliveira LE. Plasmon polaritons in photonic metamaterial Fibonacci superlattices. *Phys Rev B* 2010;81:153101.
- [71] Bruno-Alfonso A, Reyes-Gómez E, Cavalcanti SB, Oliveira LE. Unfolding of plasmon-polariton modes in one-dimensional layered systems containing anisotropic left-handed materials. *Phys Rev B* 2011;84:113101.
- [72] Shadrivov IV, Sukhorukov AA, Kivshar YS. Guided modes in negative-refractive-index waveguides. *Phys Rev E* 2003;67:057602.
- [73] Shadrivov IV, Sukhorukov AA, Kivshar YS. Complete band gaps in one-dimensional left-handed periodic structures. *Phys Rev Lett* 2005;95:193903.

- [74] Sun SL, Huang XQ, Zhou L. Two-dimensional complete photonic gaps from layered periodic structures containing anisotropic left-handed metamaterials. *Phys Rev E* 2007;75:066602.
- [75] Pendry JB, Ramakrishna SA. Focusing light using negative refraction. *J Phys: Condens Matter* 2003;15:6345–64.
- [76] Alù A, Silveirinha MG, Salandrino A, Engheta N. Epsilon-near-zero (ENZ) metamaterials and electromagnetic sources: tailoring the radiation phase pattern. *Phys Rev B* 2007;75:155410.
- [77] Ziolkowski RW. Propagation in and scattering from a matched metamaterial having a zero index of refraction. *Phys Rev E* 2004;70:046608.
- [78] Enoch S, Tayeb G, Sabouroux P, Guérin N, Vincent P. A metamaterial for directive emission. *Phys Rev Lett* 2002;89:213902.
- [79] Silveirinha M, Engheta N. Tunneling of electromagnetic energy through subwavelength channels and bends using  $\epsilon$ -near-zero materials. *Phys Rev Lett* 2006;97:157403.
- [80] Silveirinha M, Engheta N. Design of matched zero-index metamaterials using nonmagnetic inclusions in epsilon-near-zero media. *Phys Rev B* 2007;75:075119.
- [81] Silveirinha M, Engheta N. Theory of supercoupling, squeezing wave energy, and field confinement in narrow channels and tight bends using  $\epsilon$ -near-zero metamaterials. *Phys Rev B* 2007;76:245109.
- [82] Liu R, Cheng Q, Hand T, Mock JJ, Cui TJ, Cummer SA, Smith DR. Experimental demonstration of electromagnetic tunneling through an epsilon-near-zero metamaterial at microwave frequencies. *Phys Rev Lett* 2008;100:023903.
- [83] Edwards B, Alù A, Young ME, Silveirinha M, Engheta N. Experimental verification of epsilon-near-zero metamaterial coupling and energy squeezing using a microwave waveguide. *Phys Rev Lett* 2008;100:033903.
- [84] Halterman K, Feng S. Resonant transmission of electromagnetic fields through subwavelength zero- $\epsilon$  slits. *Phys Rev A* 2008;78:021805(R).
- [85] Hao JM, Yan W, Qiu M. Super-reflection and cloaking based on zero index metamaterial. *Appl Phys Lett* 2010;96:101109.
- [86] Nguyen VC, Chen L, Halterman K. Total transmission and total reflection by zero index metamaterials with defects. *Phys Rev Lett* 2010;105:233908.
- [87] Jin Y, He S. Enhancing and suppressing radiation with some permeability-near-zero structures. *Opt Express* 2010;18:16587–93.
- [88] Xu Y, Chen H. Total reflection and transmission by epsilon-near-zero metamaterials with defects. *Appl Phys Lett* 2011;98:113501.
- [89] Rahm M, Schurig D, Roberts DA, Cummer SA, Smith DR, Pendry JB. Design of electromagnetic cloaks and concentrators using form-invariant coordinate transformations of Maxwell's equations. *Photonics Nanostruct Fundam Appl* 2008;6:87–95.
- [90] Yang T, Chen HY, Luo XD, Ma HR. Superscatterer: enhancement of scattering with complementary media. *Opt Express* 2008;16:18545–50.
- [91] Chen HY, Chan CT. Transformation media that rotate electromagnetic fields. *Appl Phys Lett* 2007;90:241105.
- [92] Huang X, Lai Y, Hang ZH, Zheng H, Chan CT. Dirac cones induced by accidental degeneracy in photonic crystals and zero-refractive-index materials. *Nature Mater* 2011;10:582–6.
- [93] Gabrielli LH, Cardenas J, Poitras CB, Lipson M. Silicon nanostructure cloak operating at optical frequencies. *Nature Photon* 2009;3:461–3.
- [94] Wang LG, Wang ZG, Zhang JX, Zhu SY. Realization of Dirac point with double cones in optics. *Opt Lett* 2009;34:1510–2.
- [95] Novoselov KS, Geim AK, Morozov SV, Jiang D, Katsnelson MI, Grigorieva IV, Dubonos SV, Firsov AA. Two-dimensional gas of massless Dirac fermions in graphene. *Nature* 2005;438:197–200.
- [96] Zhang Y, Tan YW, Stormer HL, Kim P. Experimental observation of the quantum Hall effect and Berry's phase in graphene. *Nature* 2005;438:201–4.
- [97] Katsnelson MI, Novoselov KS, Geim AK. Chiral tunnelling and the Klein paradox in graphene. *Nature Phys* 2006;2:620–5.
- [98] Haldane FDM, Raghu S. Possible realization of directional optical waveguides in photonic crystals with broken time-reversal symmetry. *Phys Rev Lett* 2008;100:013904.
- [99] Zhang X, Liu Z. Extremal transmission and beating effect of acoustic waves in two-dimensional sonic crystals. *Phys Rev Lett* 2008;101:264303.
- [100] Wu Y, Li J, Zhang ZQ, Chan CT. Effective medium theory for magnetodielectric composites: beyond the long-wavelength limit. *Phys Rev B* 2006;74:085111.

Received July 7, 2012; accepted November 1, 2012